JCB Journal of Cell Biology

ARTICLE

α-Integrins dictate distinct modes of type IV collagen recruitment to basement membranes

Ranjay Jayadev[1,2], Qiuyi Chi[1], Daniel P. Keeley[1], Eric L. Hastie[1], Laura C. Kelley[1], and David R. Sherwood[1,2]

Basement membranes (BMs) are cell-associated extracellular matrices that support tissue integrity, signaling, and barrier properties. Type IV collagen is critical for BM function, yet how it is directed into BMs in vivo is unclear. Through live-cell imaging of endogenous localization, conditional knockdown, and misexpression experiments, we uncovered distinct mechanisms of integrin-mediated collagen recruitment to *Caenorhabditis elegans* postembryonic gonadal and pharyngeal BMs. The putative laminin-binding αINA-1/βPAT-3 integrin was selectively activated in the gonad and recruited laminin, which directed moderate collagen incorporation. In contrast, the putative Arg-Gly-Asp (RGD)-binding αPAT-2/βPAT-3 integrin was activated in the pharynx and recruited high levels of collagen in an apparently laminin-independent manner. Through an RNAi screen, we further identified the small GTPase RAP-3 (Rap1) as a pharyngeal-specific PAT-2/PAT-3 activator that modulates collagen levels. Together, these studies demonstrate that tissues can use distinct mechanisms to direct collagen incorporation into BMs to precisely control collagen levels and construct diverse BMs.

Introduction

Basement membrane (BM) is a thin, dense sheet of extracellular matrix that underlies epithelia and endothelia and surrounds most other tissues (Pozzi et al., 2017). BMs are comprised primarily of two independent self-assembling scaffolds of laminin and type IV collagen. The laminin and type IV collagen networks are thought to associate through several cross-bridging molecules, including nidogen, perlecan, and agrin (Yurchenco, 2011). BMs are highly diverse, and this diversity arises from alternative splicing, post-translational modifications, and varying amounts of core BM components as well as numerous regulatory proteins that associate with BMs such as matricellular proteins, proteases, and growth factors (Glentis et al., 2014; Isabella and Horne-Badovinac, 2015). The diversity in BMs regulates key cell and tissue properties, including cell polarity, cell differentiation, cell survival, tissue shaping, filtration, and resistance to mechanical stresses (Breitkreutz et al., 2013). How diverse BMs are constructed on tissues is not well understood, particularly as many BM components are expressed and secreted from distant sources and selectively acquired from the extracellular fluid (Glentis et al., 2014; Clay and Sherwood, 2015).

Type IV collagen is highly conserved among animals, and its origination in unicellular ancestors was thought to have been a requirement for the formation of BMs and appearance of complex tissues in animals (Grau-Bové et al., 2017; Fidler et al., 2018). Type IV collagen is a heterotrimer made up of two α1-like and one α2-like chains that wind around each other into a long and rigid 400-nm triple helix. Vertebrates harbor three α1-like and three α2-like chains and construct three distinct heterotrimers (Khoshnoodi et al., 2008). The stiff triple-helical structure together with covalent cross-linking between type IV collagen molecules gives BMs mechanical resistance to tensile forces (Fidler et al., 2018). In addition to providing structural integrity, type IV collagen networks function as molecular scaffolds that bind other BM components, growth factors, and extracellular enzymes (Wang et al., 2008; Parkin et al., 2011; Brown et al., 2017). Furthermore, distinct levels, unique modes of deposition, and targeted remodeling of collagen within BMs helps shape organs (Gupta et al., 1997; Pöschl et al., 2004; Harunaga et al., 2014; Isabella and Horne-Badovinac, 2016; Crest et al., 2017). Highlighting its importance to human health, mutations in type IV collagen are associated with at least 10 distinct genetic disorders that disrupt brain, kidney, muscle, and vascular tissues (Fidler et al., 2018). In mice, *Drosophila melanogaster*, and *Caenorhabditis elegans*, type IV collagen is often secreted by cells into the extracellular space and then incorporated into epithelial BMs at distant sites (Graham et al., 1997; Kedinger et al., 1998; Pastor-Pareja and Xu, 2011). Work in *Drosophila* and mouse embryos have indicated that type IV collagen recruitment to BMs requires the presence of laminin (Pöschl et al., 2004; Urbano et al., 2009; Matsubayashi et al.,

[1]Department of Biology, Regeneration Next, Duke University, Durham, NC; [2]Department of Pharmacology and Cancer Biology, Duke University, Durham, NC.

Correspondence to David R. Sherwood: david.sherwood@duke.edu.

2017). Cell culture work has suggested that laminin deposition onto cell surfaces is mediated through interactions with integrin and dystroglycan receptors, and with sulfated glycolipids (Li et al., 2005, 2017; Yurchenco, 2011). The cell surface mechanisms that mediate laminin and collagen deposition in vivo, however, remain elusive. Further, while most studies have examined initial BM formation in the embryo, little is known about BM construction on growing tissues, where most BMs are found.

Many factors have limited the study of how BMs are constructed and the mechanisms by which type IV collagen is deposited into them. Laminin and type IV collagen are essential for embryonic animal development, hindering postembryonic studies. Further, in vertebrates there are three distinct type IV collagens, 16 laminins, and at least 24 integrin αβ heterodimer receptors, making interpretation of genetic analysis daunting (Clay and Sherwood, 2015). In addition, BM components and receptors have not yet been tagged in vertebrates with genetically encoded fluorescent proteins to dynamically examine their localization (Kelley et al., 2014). *C. elegans* is a powerful model system to address many of these experimental limitations. Type IV collagen and laminin, as well as many BM-interacting receptors, have been functionally tagged with fluorescent proteins (Hagedorn et al., 2009; Ihara et al., 2011; McClatchey et al., 2016). Further, core BM matrix components and receptors are conserved in the worm but have not undergone the dramatic gene family expansion found in vertebrates. For example, *C. elegans* has only a single type IV collagen, two laminins, and two integrin heterodimers. Finally, RNAi can be used to conditionally knock down BM components postembryonically to avoid early lethality (Clay and Sherwood, 2015).

In this work, we examined the mechanism of type IV collagen addition into the growing BMs covering two organs during *C. elegans* larval development: the pharynx, a rigid pumping feeding organ, and the gonad, a flexible cylindrical organ that houses the germline. Using RNAi-mediated knockdown and an mCherry-tagged type IV collagen reporter, we found that collagen addition to BM was required to maintain both organs' structure, and that the pharyngeal BM contained significantly higher collagen levels. Strikingly, while laminin was necessary for type IV collagen addition into the gonadal BM, collagen addition appeared to be independent of laminin in the pharyngeal BM. Through RNAi screening and examination of endogenously tagged BM-binding receptors, we discovered that the putative laminin-binding integrin heterodimer αINA-1/βPAT-3 mediated laminin and collagen addition to the gonadal BM, while the putative Arg-Gly-Asp tripeptide (RGD)-binding integrin αPAT-2/βPAT-3 (Ruoslahti, 1996) promoted collagen addition to the pharyngeal BM, which appeared to be independent of laminin. However, both integrin heterodimers were expressed in the gonad and the pharynx, suggesting that their selective activation was controlled by tissue-specific effectors. Consistent with this hypothesis, domain-swapping experiments demonstrated that the intracellular domain of the α-integrin PAT-2 drove BM recruiting activity of the INA-1 extracellular domain in the pharynx, where INA-1 is normally not active. Further, using an RNAi screen we identified RAP-3, an orthologue of the mammalian integrin-activating small GTPase Rap1, as a pharyngeal-specific activator of PAT-2/PAT-3. Together, these results identify integrin receptors as key in vivo mediators of collagen incorporation into BM during tissue growth and show that BM diversity and precise modulation of BM collagen levels can be driven in part by the tissue-specific activation of distinct integrins.

Results

The pharynx and gonad are BM-encased growing organs supported by type IV collagen

In *C. elegans*, collagen IV is a heterotrimer formed from two α1-like chains and one α2-like chain, encoded by the *emb-9* and *let-2* genes, respectively (Kramer, 2005). Collagen is predominantly synthesized in body wall muscles, secreted into the extracellular space, and then recruited to the BMs of other tissues (Graham et al., 1997; Morrissey et al., 2016). To understand how type IV collagen is targeted to the BMs of growing organs, we examined the BMs of the pharynx and the gonad (Fig. 1 A). The *C. elegans* pharynx is a rigid, contractile feeding apparatus largely composed of radially arranged muscle and marginal cells that form an epithelium (Mango, 2007). The gonad is a flexible cylindrical reproductive organ that is enwrapped predominantly by thin gonadal sheath cells (Sherwood and Plastino, 2018). The pharyngeal epithelium and gonadal sheath cells are both surrounded by BMs that support each organ (Huang et al., 2003). Using a functional type IV collagen reporter (EMB-9::mCherry [Ihara et al., 2011], referred to as collagen::mCh), we examined surface area projections of the gonadal and pharyngeal BMs and found that the pharyngeal BM grew approximately threefold in surface area during larval development (L1 through young adult), while the gonadal surface area increased >90-fold (Fig. 1 B). To determine if type IV collagen addition was required to maintain BM and tissue integrity during pharynx and gonad growth, we depleted EMB-9 protein (α1-like chain) by RNAi beginning at the L1 larval stage and analyzed both organs at adulthood (48 h and 72 h, Fig. 1 A). We found that reduction of EMB-9 frequently resulted in deformation of the anterior pharyngeal bulb (n = 15/20 72-h adult animals, Fig. 1 C), and severe distortion and rupturing of gonadal tissue (n = 20/20 48-h young adult animals, Fig. 1 C). Similar results were observed upon RNAi knockdown of *let-2* (the α2-like chain of collagen IV, n = 17/20 animals with anterior pharyngeal bulb deformation and n = 20/20 animals with gonadal rupturing). Linescan analysis of mean fluorescence intensity revealed an ∼70% reduction in collagen::mCh levels in the pharyngeal BM. Further, gaps in collagen signal appeared at regions of pharyngeal bulb deformation (Fig. 1 C). Collagen was reduced by ∼60% in the gonad at the early L3 stage, before BM rupturing and the gonadal tissue became disorganized (Fig. 1 C). Taken together, these results indicate that addition of type IV collagen to the BM is necessary to maintain tissue integrity during pharyngeal and gonadal growth.

The pharyngeal BM is collagen rich, but laminin poor, compared with the gonadal BM

BMs of different tissues often vary in levels and composition of matrix components (Halfter et al., 2015; Randles et al., 2017). To

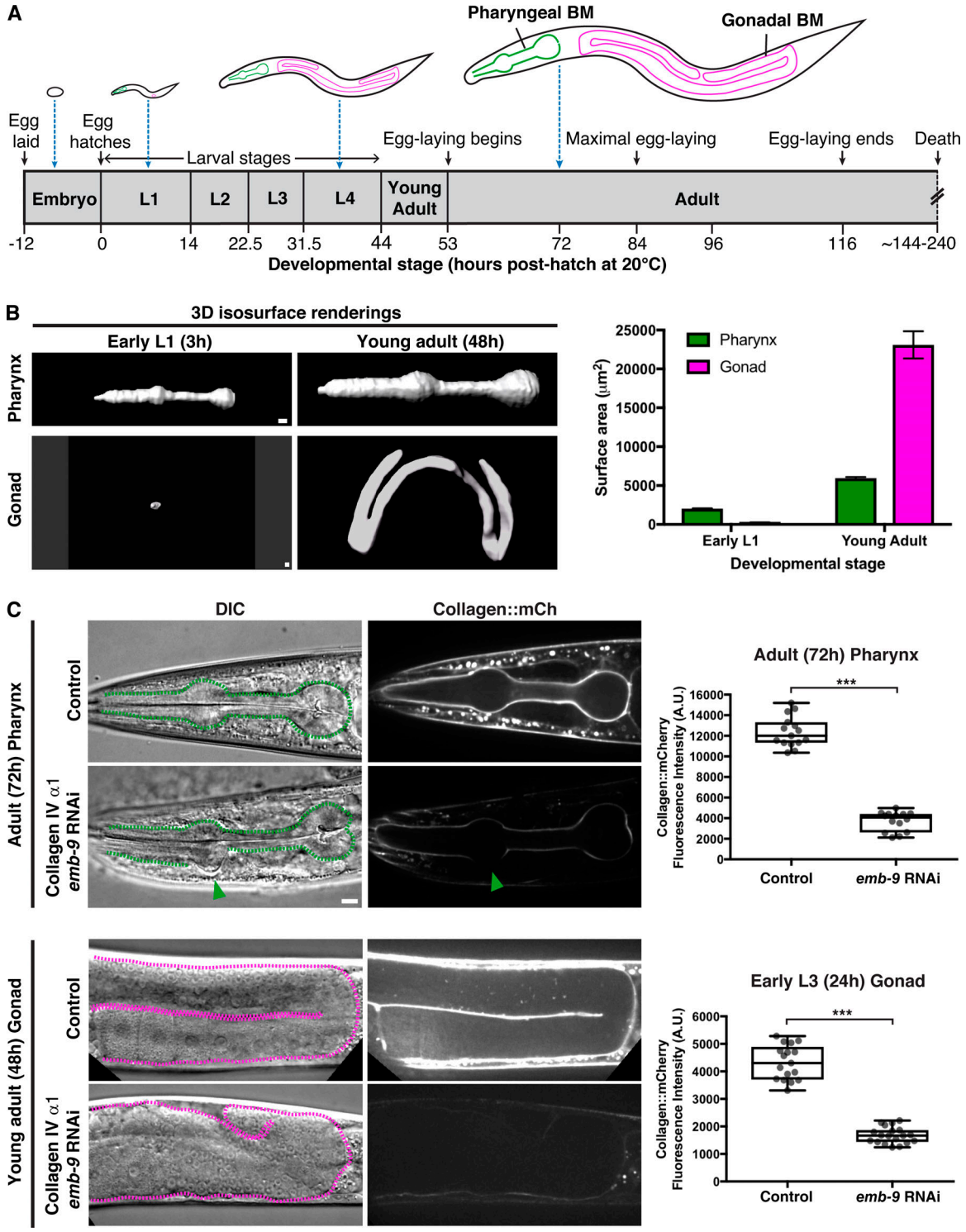

Figure 1. **BM type IV collagen supports the growing *C. elegans* pharynx and gonad. (A)** Illustrations of *C. elegans* at various stages of development (scaled to the length of the egg), with the pharyngeal and gonadal BMs outlined in green and magenta, respectively. **(B)** 3D isosurface renderings of pharyngeal and gonadal type IV collagen::mCh at the early L1 versus young adult stages on the left, and quantification of surface area on the right. Bar graphs show mean surface area, and error bars represent standard error of the mean (n = 10 all stages). **(C)** DIC and collagen::mCh fluorescence images of 72-h adult pharynxes (top left) and 48-h young adult gonads (bottom left) of control (L4440 empty vector) and collagen IV α1 (*emb-9*) RNAi-treated animals. Pharynxes in DIC images (top left) are outlined with green dotted lines. The green arrowhead indicates a deformation in the anterior pharyngeal bulb, corresponding to a region with undetectable collagen::mCh signal. Mean pharyngeal BM collagen::mCh fluorescence intensity in control (n = 15) and *emb-9* RNAi-treated (n = 14) 72-h adult animals are quantified on the top right. Dotted magenta lines outline gonads in DIC images (bottom left). The gonads of *emb-9* RNAi-treated animals are severely misshapen, correlating with near-undetectable BM collagen::mCh signal. Mean gonadal BM collagen::mCh fluorescence intensity in control (n = 17) and *emb-9* RNAi-treated (n = 19) early L3 animals are quantified on the bottom right. ***, P < 0.0001, unpaired two-tailed Student's t test. Box edges in boxplots depict the 25th and 75th percentiles, the line in the box indicates the median value, and whiskers mark the minimum and maximum values. Scale bars, 10 µm. A.U., arbitrary units.

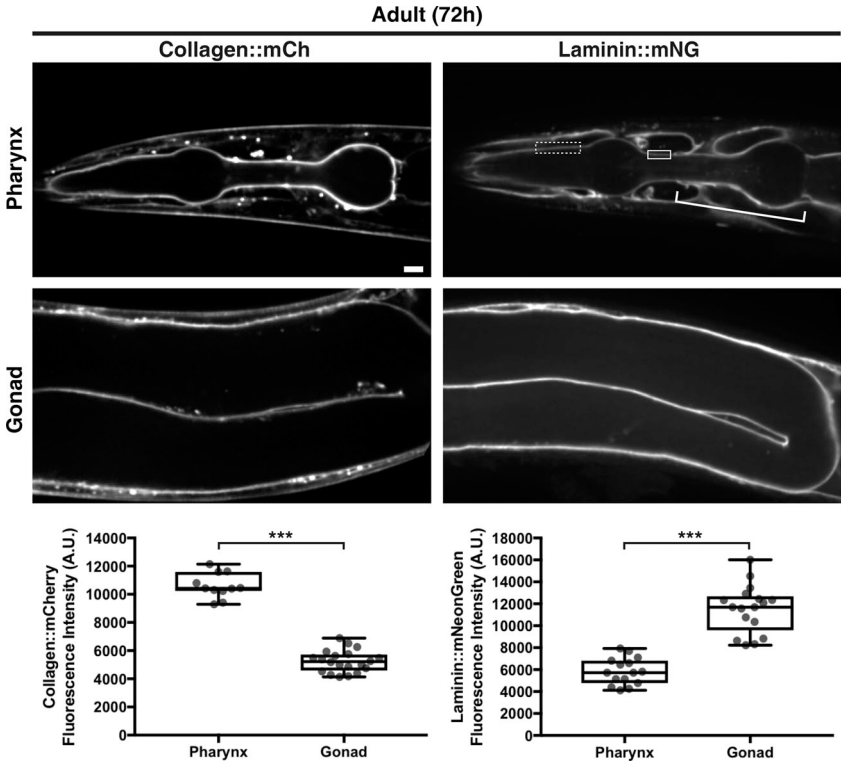

Figure 2. **The pharyngeal BM is collagen rich, while the gonadal BM is laminin rich.** Fluorescence images of collagen::mCh and laminin::mNG in the pharynx and gonad of 72-h adult animals. As laminin::mNG localizes strongly to the nerve ring BM that surrounds and contacts the pharyngeal BM at several regions (bracket), we confined our measurements of laminin signal to the dotted box where clear pharyngeal BM laminin is visible in this and all relevant figures, except Fig. 6 C, where laminin signal in the solid box was also measured. Quantification of collagen::mCh and laminin::mNG levels in the pharyngeal (collagen::mCh, n = 11; laminin::mNG, n = 15) and gonadal BMs (collagen::mCh, n = 20; laminin::mNG, n = 17) are shown in boxplots at the bottom. ***, $P < 0.0001$, unpaired two-tailed Student's t test. Box edges in boxplots depict the 25th and 75th percentiles, the line in the box indicates the median value, and whiskers mark the minimum and maximum values. Scale bar, 10 µm. A.U., arbitrary units.

determine if type IV collagen levels differ between the gonadal and pharyngeal BMs, we quantified collagen::mCh fluorescence intensity in both organs and found that collagen was present at twofold higher levels in the pharyngeal BM versus the gonadal BM in 72-h adults (Fig. 2). As embryonic studies have suggested that collagen is recruited to BMs through association with laminin networks (Huang et al., 2003; Pöschl et al., 2004; Urbano et al., 2009; Matsubayashi et al., 2017), we next analyzed BM laminin levels in the two tissues. Laminins are heterotrimers comprised of an α, β, and γ chain. *C. elegans* encodes two α subunits (*lam-3* and *epi-1*), one β subunit (*lam-1*), and one γ subunit (*lam-2*) that form two distinct laminin heterotrimers (Kramer, 2005). To assess laminin levels in the BM, we used CRISPR/Cas9 to encode *mNeonGreen* at the *lam-2* genomic locus, generating worms expressing the LAM-2::mNG fusion protein (referred to as laminin::mNG). We found that there were twofold lower levels of laminin in the pharyngeal BM compared with the gonadal BM (Fig. 2). Thus, there are higher levels of type IV collagen and lower levels of laminin in the pharyngeal BM compared with the gonadal BM.

Laminin is required for collagen recruitment to the gonadal but not pharyngeal BM

The differences in collagen and laminin levels in the adult pharyngeal and gonadal BMs suggested that the interaction between type IV collagen and laminin may differ in the BMs of these tissues. The early deposition of laminin is essential for polarizing the nascent pharyngeal epithelium during embryonic development, and for the addition of type IV collagen and perlecan during late embryogenesis (Rasmussen et al., 2012). We next asked whether laminin was required to recruit collagen to the postembryonic BMs of the pharynx and the gonad during larval development. We used RNAi to deplete LAM-2 (the sole laminin γ subunit) beginning in the L1 larval stage and analyzed BM collagen levels during subsequent larval development and adulthood. By the early L3 larval stage (24-h RNAi treatment), there was an ∼50% reduction in gonadal BM laminin levels (Fig. S1 A), correlating with a similar reduction in type IV collagen levels (Fig. 3 A). Breaks in the BM were observed shortly after this time (∼26-h RNAi treatment, n = 12/20 animals), followed by BM rupturing (mid L4, Fig. 3 A, n = 20/20 worms), and ultimately gonadal tissue disintegration (72-h adult, Fig. 3 A, n = 20/20 animals examined). In contrast, the pharyngeal BM collagen levels increased (similar to control animals) despite a strong knockdown of laminin (∼70% reduction in laminin levels by 96-h adult, Figs. 3 B and S1 B), and there were no defects in pharyngeal structure (n = 14/14 animals). These observations suggest that type IV collagen recruitment to the growing BM might be distinct in each tissue: laminin dependent in the gonad but possibly laminin independent in the pharynx.

INA-1/PAT-3 integrin mediates collagen recruitment to the gonadal BM in a laminin-dependent manner

Work in cell culture has suggested that interactions with laminin-binding integrin and dystroglycan receptors as well as cell surface sulfated glycolipids might seed laminin polymerization to initiate BM assembly, leading to subsequent collagen recruitment (Yurchenco and Patton, 2009; Li et al., 2017). Because of possible redundancy between these mechanisms and within the large integrin gene family in vertebrates, however, there has not yet been clear genetic evidence for any of these mechanisms in regulating laminin and collagen recruitment to

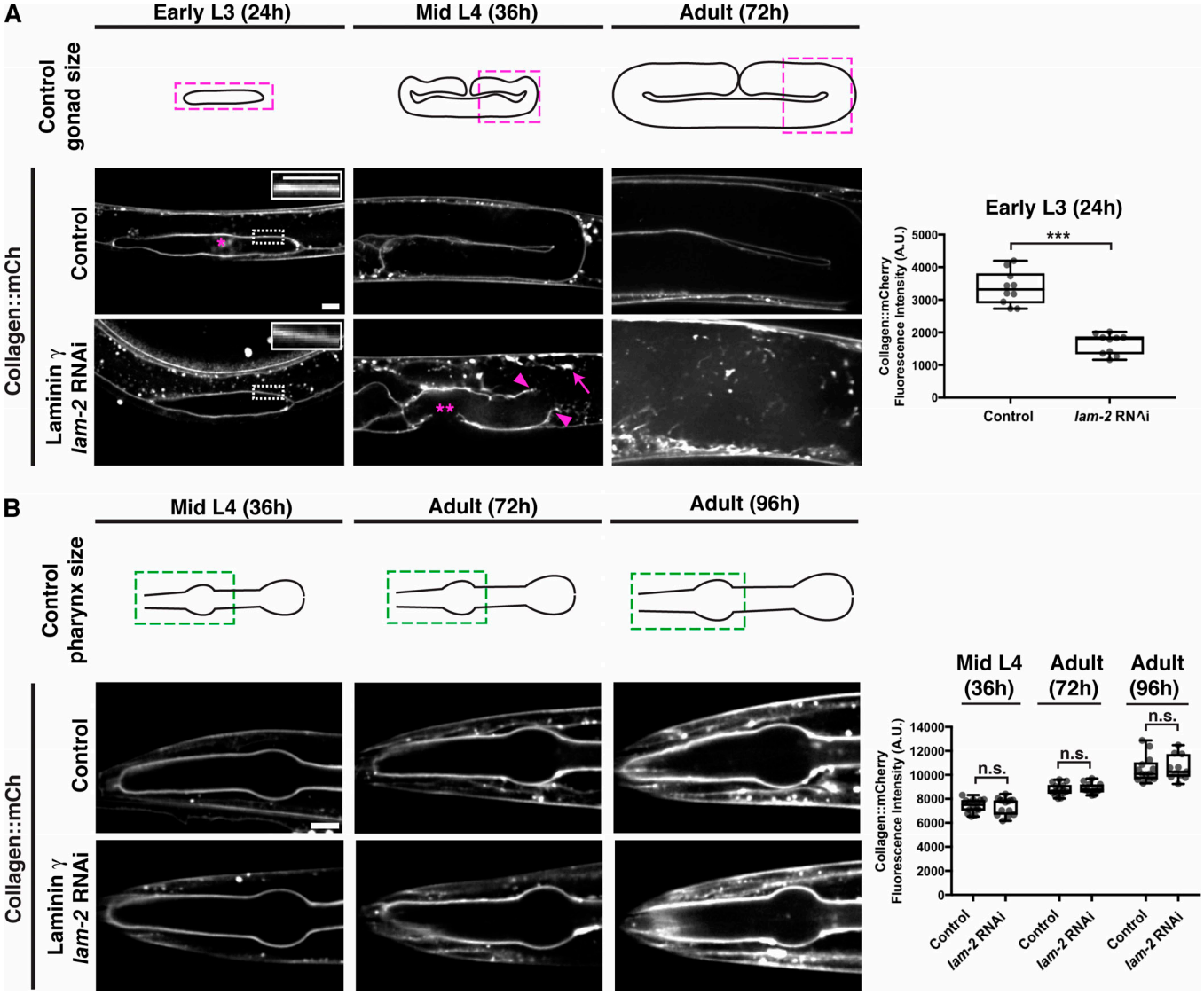

Figure 3. **Collagen recruitment to the gonadal but not pharyngeal BM is dependent on laminin. (A)** Fluorescence images of gonadal BM collagen::mCh shown at the early L3, mid-L4, and 72-h adult stages in control and laminin γ (*lam-2*) RNAi-treated animals (RNAi fed at the L1 stage onwards). Control gonad size at these stages are shown in schematics, and the magenta boxes denote regions of the gonad shown in the figure. Collagen::mCh signal in the dotted box regions are magnified in insets. The asterisk indicates non-BM collagen::mCh signal from coelomocytes. Gonadal BM collagen::mCh fluorescence intensity in control (n = 10) and *lam-2* (n = 10) RNAi-treated early L3 animals is quantified on the right. By the mid-L4 stage, rupturing of the gonadal BM (magenta arrowheads) and abnormal collagen aggregation (magenta arrow) was observed in *lam-2* RNAi-treated animals (n = 20/20). The double asterisks mark a break in the BM due to anchor cell invasion, a normal morphogenetic event during *C. elegans* vulval development. **(B)** Fluorescence images of pharyngeal BM collagen::mCh in control and *lam-2* RNAi-treated animals shown at the mid L4, 72-h adult, and 96-h adult stages. Control pharynx size at these stages are shown in schematics, and the green boxes denote regions of the pharynx shown in the figure. Pharyngeal BM collagen::mCh fluorescence intensity in control and *lam-2* RNAi-treated animals at all three stages are quantified on the right (mid L4 control, n = 14; *lam-2* RNAi, n = 14; 72-h adult control, n = 14; *lam-2* RNAi, n = 12; 96-h adult control, n = 13; *lam-2* RNAi, n = 11). ***, $P < 0.0001$, unpaired two-tailed Student's t test; n.s. (not significant), $P > 0.05$. Box edges in boxplots depict the 25th and 75th percentiles, the line in the box indicates the median value, and whiskers mark the minimum and maximum values. Scale bars, 10 µm. A.U., arbitrary units.

BMs in vivo (Yurchenco, 2015). As C. *elegans* does not synthesize sulfated glycolipids (Bai et al., 2018), we hypothesized that tissue-specific roles for integrin and dystroglycan might explain the different modes of collagen recruitment to the pharyngeal and gonadal BMs.

To investigate the cell surface interactions that recruit type IV collagen to developing tissues, we initially focused on the gonadal BM. We first examined the dystroglycan receptor. *C. elegans* harbors a single vertebrate dystroglycan orthologue, *dgn-1* (Johnson et al., 2006). Endogenously tagged DGN-1::mNG (Naegeli et al., 2017) was expressed in the gonad and localized to the gonad–BM interface (Fig. S2 A). Knockdown of *dgn-1* by RNAi eliminated detectable DGN-1::mNG but did not affect either laminin or collagen levels in adult animals (Fig. S2 B). We next investigated the integrin receptor system. *C. elegans* assembles two integrin heterodimers, composed of the α subunits

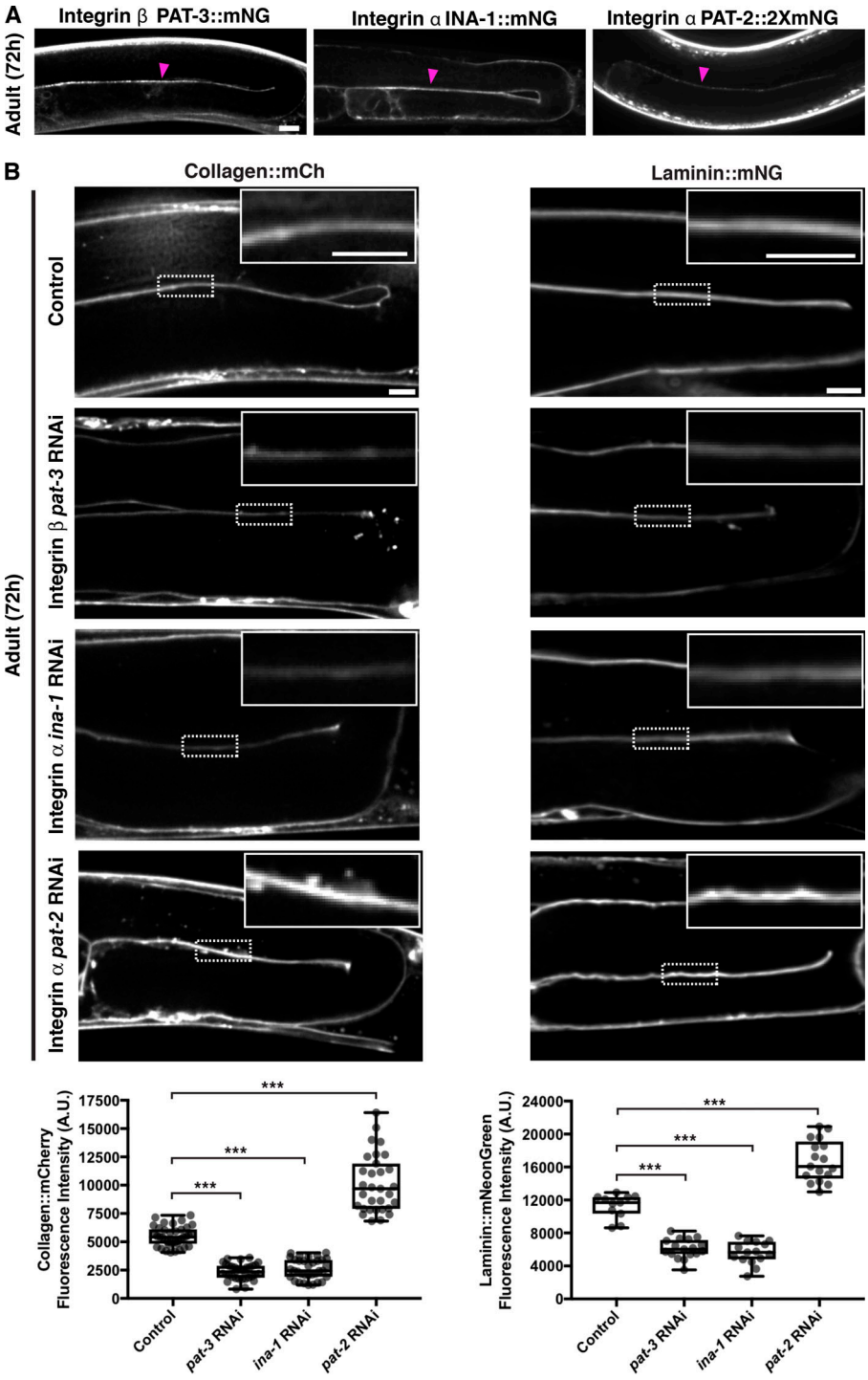

Figure 4. **The INA-1/PAT-3 integrin heterodimer is required for laminin-dependent collagen recruitment to the gonadal BM. (A)** Fluorescence images of the integrin β subunit PAT-3::mNG and the integrin α subunits INA-1::mNG and PAT-2::2xmNG in the gonad. Magenta arrowheads indicate enrichment of fluorescence signal at the cell–BM interface. **(B)** Fluorescence images of gonadal BM collagen::mCh (left) and laminin::mNG (right) in control versus *pat-3*, *ina-1*, and *pat-2* RNAi-treated 72-h adult animals. Regions of the BM in the dotted boxes are magnified in insets. Quantification of collagen::mCh (control, $n = 38$; *pat-3* RNAi, $n = 34$; *ina-1* RNAi, $n = 34$; *pat-2* RNAi, $n = 31$) and laminin::mNG (control, $n = 11$; *pat-3* RNAi, $n = 17$; *ina-1* RNAi, $n = 15$; *pat-2* RNAi, $n = 17$) fluorescence intensity for all treatments is shown at the bottom. ***, $P < 0.0001$, one-way ANOVA followed by post hoc Dunnett's test. Box edges in boxplots depict the 25th and 75th percentiles, the line in the box indicates the median value, and whiskers mark the minimum and maximum values. Scale bars, 10 µm. A.U., arbitrary units.

PAT-2 (most similar to RGD-binding integrins) or INA-1 (most similar to laminin-binding integrins) dimerized to the sole β subunit PAT-3 (Kramer, 2005). Endogenously tagged INA-1::mNG, PAT-2::2XmNG, and PAT-3::mNG were expressed in the gonad and localized to the cell–BM interface (Fig. 4 A). L1 RNAi-mediated knockdown of *ina-1* and *pat-3* each resulted in an ∼50% reduction in collagen::mCh levels in adult animals (Figs. 4 B and S3 A), suggesting that the INA-1/PAT-3 integrin heterodimer is required for type IV collagen recruitment to the gonadal BM. Importantly, RNAi against *ina-1* and *pat-3* did not appear to alter collagen secretion from the muscle cells (Fig. S3 B), suggesting a local collagen-recruiting function for INA-1/PAT-3 in the gonad. As gonadal BM collagen localization is dependent on laminin, we analyzed laminin::mNG levels upon *ina-1* and *pat-3* knockdown and found a similar ∼50% reduction (Fig. 4 B) in each condition. Surprisingly, depletion of the other integrin α subunit PAT-2 by RNAi yielded an increase in BM collagen and laminin levels (Figs. 4 B and S3 A). We speculated that this could be due to more INA-1/PAT-3 heterodimers forming upon reduction of PAT-2. Consistent with this, RNAi against *pat-2* more than doubled

INA-1::mNG levels at cell surfaces contacting the gonadal BM (Fig. S3 C).

To determine if any other matrix receptors contribute to collagen recruitment to the gonadal BM, we performed RNAi against worm orthologues of glypican (*gpn-1* and *lon-2*), leukocyte common antigen-related receptor protein tyrosine phosphatase (*ptp-3*), teneurin (*ten-1*), and discoidin domain receptors (*ddr-1* and *ddr-2*; Kramer, 2005). Knockdown of these receptors did not affect gonadal collagen levels (Fig. S3 D). Taken together, our findings suggest that the putative laminin-binding INA-1/PAT-3 integrin heterodimer is the predominant cell surface receptor that mediates collagen IV recruitment to the gonadal BM through a laminin-dependent mechanism.

The PAT-2/PAT-3 integrin heterodimer promotes collagen recruitment to the pharyngeal BM independent of laminin

We next sought to determine the cell surface receptors mediating collagen recruitment to the pharyngeal BM. DGN-1::mNG expression was not detectable in the pharynx (Fig. S4 A). In contrast, all three integrin subunits were present in the pharyngeal epithelium and localized to the pharynx–BM interface (Fig. 5 A). RNAi against *ina-1* did not affect pharyngeal BM collagen or laminin levels (96 h RNAi treatment, Figs. 5 B and S4 B). However, RNAi targeting *pat-2* and *pat-3* each reduced pharyngeal BM collagen levels by >40% (Figs. 5 B and S4 B). Notably, RNAi against *pat-2* or *pat-3* did not affect pharyngeal BM laminin levels (Fig. 5 B). These results suggest that the PAT-2/PAT-3 integrin promotes pharyngeal BM collagen recruitment independent of laminin. To determine whether PAT-2 is sufficient to recruit collagen to the pharyngeal BM, we overexpressed PAT-2::mNG specifically in pharyngeal muscle cells by using the *myo-2* promoter and mosaic extrachromosomal array expression (Fig. 5 C). Analysis of mosaic overexpression in adult animals revealed that pharyngeal BM collagen::mCh levels were increased by ∼30% in regions where PAT-2 was overexpressed (Fig. 5 C). Finally, RNAi-mediated reduction of other major matrix receptors did not affect collagen levels in the pharyngeal BM (Fig. S4 C). Together, these observations indicate that the putative RGD-binding PAT-2/PAT-3 integrin heterodimer is the predominant cell surface receptor that is required and sufficient to mediate type IV collagen recruitment to the pharyngeal BM independent of laminin. Further, these results suggest that the recruitment of laminin to the growing pharyngeal BM is not dependent on integrins (either INA-1/PAT-3 or PAT-2/PAT-3) but is mediated by an unknown mechanism.

The PAT-2 intracellular domain dictates BM recruiting activity of integrins in the pharynx

All integrin subunits were expressed in both the gonadal and pharyngeal tissues. Thus, we next sought to determine the mechanism controlling the tissue-specific activity of the two integrin heterodimers in matrix recruitment. Recent studies have suggested that the diverse intracellular C-terminal membrane-distal (CTMD) regions of vertebrate α-integrins may provide specificity for integrin inside-out activation, a form of integrin activation where intracellular regulators bind the cytoplasmic tails of integrin heterodimers and trigger conformational changes that allow high-affinity binding of the integrin extracellular domain with matrix ligands (Thinn et al., 2018). As the sole difference between INA-1/PAT-3 and PAT-2/PAT-3 integrin heterodimers is the α subunit, we speculated that their tissue-specific activity in collagen recruitment could be regulated by their distinct α-integrin intracellular domains mediating inside-out activation. Indeed, INA-1 and PAT-2 diverge significantly in their CTMD regions (Fig. 6 A).

Building off of these studies, and our findings that INA-1/PAT-3 integrin is expressed in the pharynx but does not recruit laminin to the pharyngeal BM, we hypothesized that the pharynx-active intracellular domain of PAT-2 fused to the laminin-binding extracellular domain of INA-1 might be able to recruit laminin in this tissue. We engineered animals that express this chimeric α-integrin subunit in the pharynx (*myo-2p*::INA-1[EX]::PAT-2[CTMD]::mNG; Fig. 6 B). Mosaic overexpression of this chimeric integrin resulted in an ∼50% increase in laminin levels in regions of the BM contacting chimera-expressing pharyngeal cells (Fig. 6 C). Notably, despite increased laminin levels, BM collagen levels were unaffected (Fig. 6 D), offering further support for the laminin-independent recruitment of collagen to the BM. In addition, we hypothesized that overexpression of the reciprocal chimeric α-integrin (PAT-2[EX]::INA-1[CTMD]) or full-length INA-1 in the pharynx might outcompete PAT-2 for PAT-3 binding and thus would disrupt collagen recruitment to the pharyngeal BM. However, we could not view transgenic animals expressing these constructs in the pharynx, as they died during embryonic development or shortly after hatching. Together, our findings suggest that the cytoplasmic domain of PAT-2 facilitates the PAT-2/PAT-3–mediated recruitment of collagen to the pharyngeal BM and when attached to the extracellular domain of INA-1 triggers laminin recruitment instead.

RAP-3 is a pharyngeal-specific activator of PAT-2/PAT-3 integrin

Our results suggested that there might be tissue-specific factors that activate PAT-2/PAT-3 in the pharynx via the PAT-2 intracellular domain to mediate BM matrix recruitment. Proteomic, localization, and genetic screening approaches have identified numerous proteins that localize with integrins or regulate integrin activity (Horton et al., 2016). To identify potential tissue-specific regulators of PAT-2/PAT-3 integrin-mediated collagen IV recruitment to BM, we performed a targeted RNAi screen (Table S1) of *C. elegans* orthologues of 32 known integrin-associated or regulatory proteins (Bouvard et al., 2013; Horton et al., 2015; Lilja et al., 2017). We searched for proteins whose loss reduced type IV collagen levels in the pharyngeal BM but did not affect gonadal BM collagen levels. RNAi against one gene, *rap-3*, led to an ∼40% reduction of pharyngeal type IV collagen levels without affecting gonadal BM collagen, suggesting it could be a specific activator of PAT-2/PAT-3 in the pharynx (Table S1 and Fig. 7, A and B).

The *rap-3* gene encodes a Rap-like protein most similar to the mammalian Rap1 isoforms Rap1A and Rap1B (Reiner and Lundquist, 2018). Rap1 is a member of the Ras family of small GTPases, and Rap1 has been implicated as an activator of

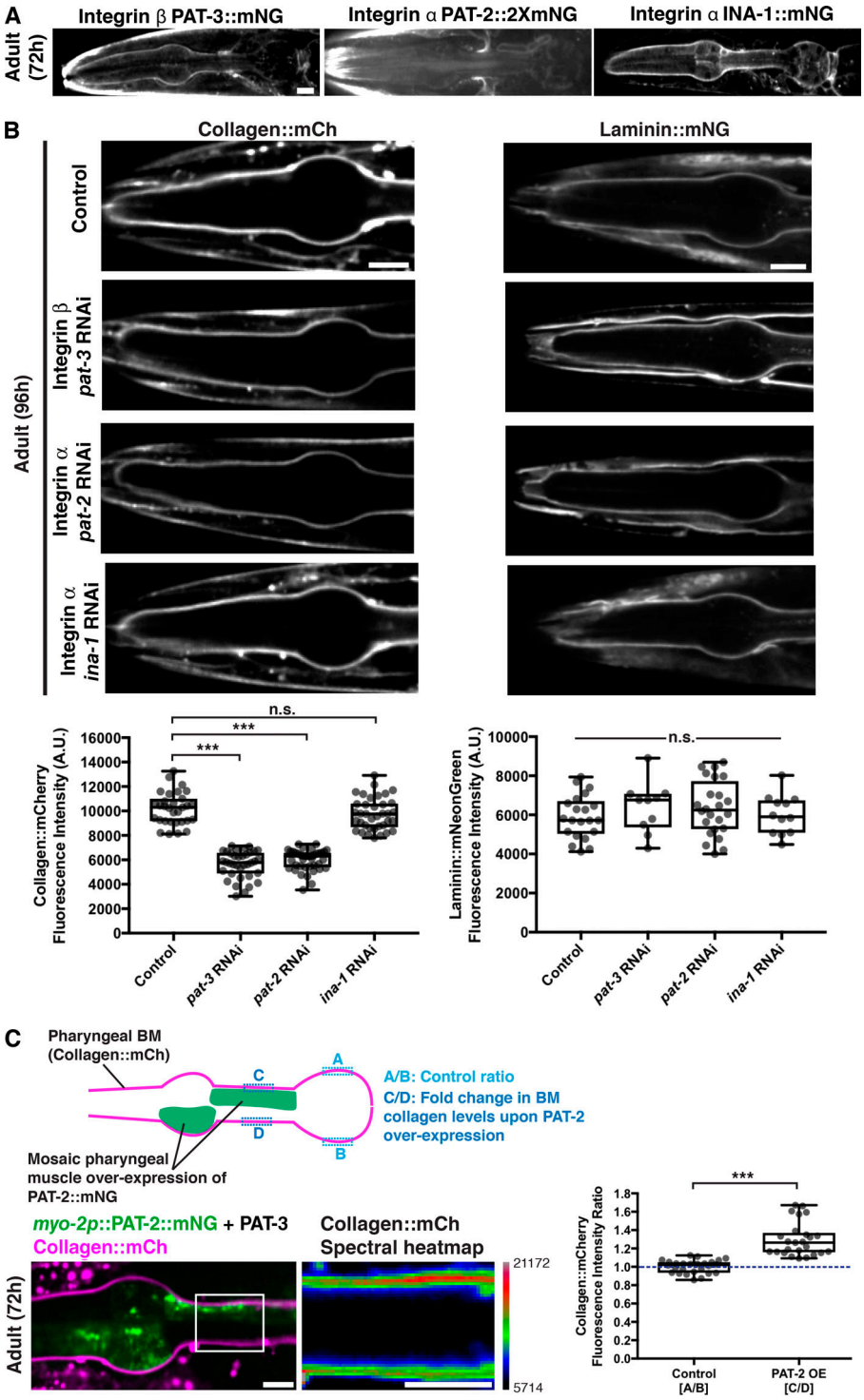

Figure 5. **The PAT-2/PAT-3 integrin heterodimer is required for laminin-independent collagen recruitment to the pharyngeal BM.** **(A)** Fluorescence images of the integrin β subunit PAT-3::mNG and the integrin α subunits PAT-2::2xmNG and INA-1::mNG in the pharynx. **(B)** Fluorescence images of pharyngeal BM collagen::mCh (left) and laminin::mNG (right) in control versus *pat-3*, *pat-2*, and *ina-1* RNAi-treated 96-h adult animals. Quantification of collagen::mCh (control, n = 31; *pat-3* RNAi, n = 36; *pat-2* RNAi, n = 39; *ina-1* RNAi, n = 37) and laminin::mNG (control, n = 21; *pat-3* RNAi, n = 10; *pat-2* RNAi, n = 24; *ina-1* RNAi, n = 12) fluorescence intensity for all treatments is shown at the bottom. Bottom left: ***, $P < 0.0001$, one-way ANOVA followed by post hoc Dunnett's test; n.s. (not significant), $P > 0.05$. Bottom right: n.s. (not significant), $P > 0.05$, one-way ANOVA. **(C)** A schematic outlining mosaic overexpression of PAT-2::mNG in the pharyngeal muscle cells and method for quantification of collagen levels is shown on top. A merged fluorescence image of *myo-2p*::PAT-2::mNG (green) and collagen::mCh (magenta) in a 72-h adult pharynx is shown on the bottom left. A spectral heatmap of collagen::mCh fluorescence intensity in the boxed region is shown on the bottom right. Quantification of the fold change in pharyngeal BM collagen::mCh fluorescence intensity upon PAT-2 overexpression is shown on the right (n = 25). ***, $P < 0.0001$, paired two-tailed Student's t test. Box edges in boxplots depict the 25th and 75th percentiles, the line in the box indicates the median value, and whiskers mark the minimum and maximum values. Scale bars, 10 µm. A.U., arbitrary units.

integrins in numerous contexts, especially in blood and endothelial cells (Boettner and Van Aelst, 2009; Carmona et al., 2009; Lagarrigue et al., 2016). To determine if the RAP-3 protein might be a tissue-specific regulator of PAT-2/PAT-3 integrin activity, we first generated RAP-3::mNG–expressing animals using CRISPR/Cas9 genome editing. Consistent with a pharynx-specific function, we found that RAP-3::mNG was expressed in the pharynx of larval and adult animals but was not detectable in gonadal tissue (Figs. 7 C and S5 A).

We hypothesized that if RAP-3 specifically activates PAT-2/PAT-3 to recruit type IV collagen, then it would not be involved in laminin recruitment. Supporting this notion, we found that pharyngeal BM laminin levels were unaffected by RNAi targeting *rap-3* (Figs. 7 D and S5 B). Further, pharyngeal-specific overexpression of a constitutively active form of RAP-3 (RAP-3^{G12V}; Jeon et al., 2007) resulted in an ∼50% increase in collagen levels in regions of the pharyngeal BM in contact with RAP-3^{G12V}-overexpressing cells (Fig. 7 E). To test whether RAP-3 and

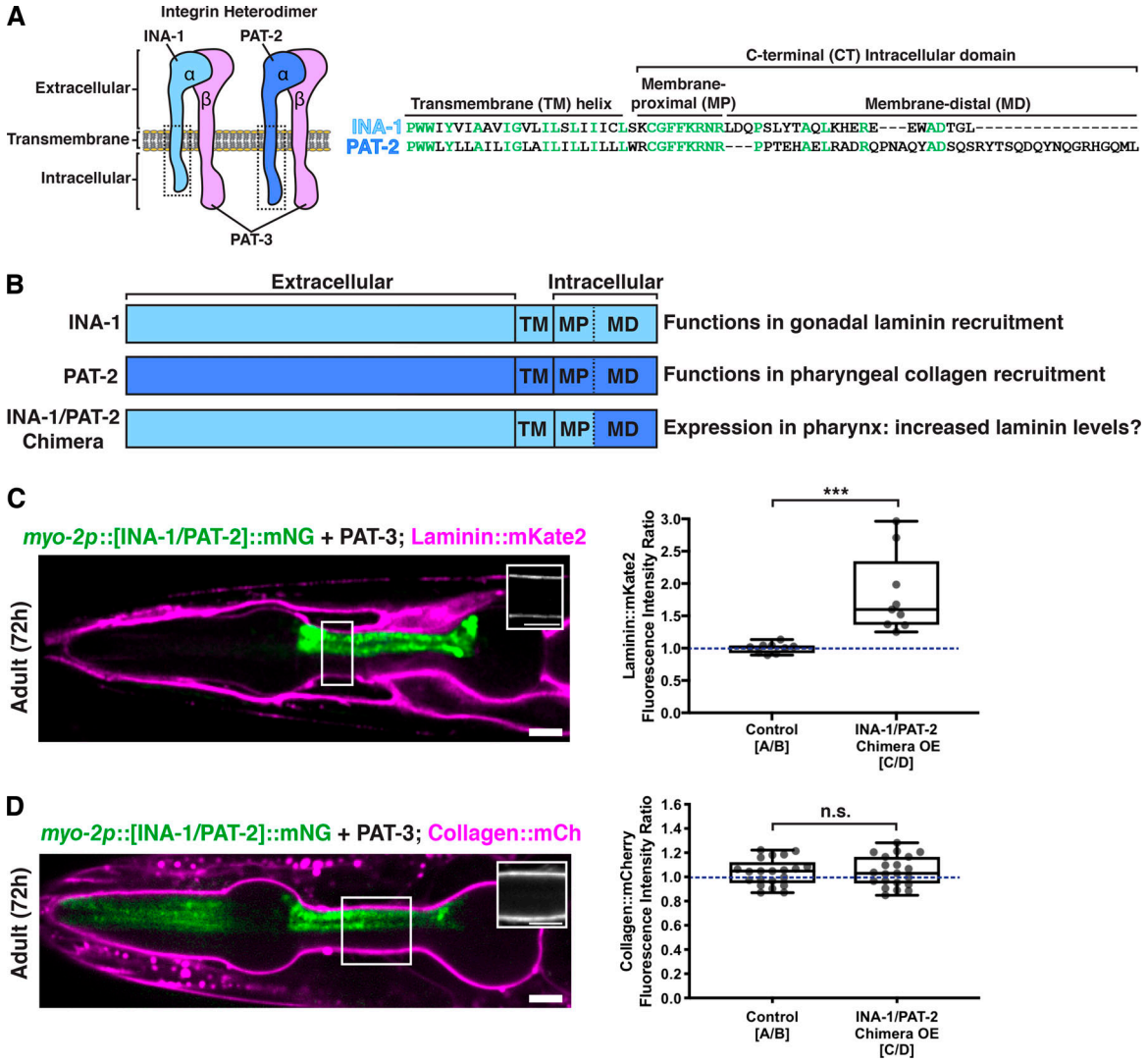

Figure 6. **The intracellular domain of PAT-2 controls the activity of PAT-2/PAT-3 in the pharynx to promote collagen recruitment independent of laminin. (A)** A schematic of the two integrin heterodimers expressed in the worm, highlighting the extracellular, transmembrane, and C-terminal intracellular regions of these proteins. Amino acid alignments of the boxed transmembrane and intracellular regions of INA-1 and PAT-2 are shown on the right. Highly conserved residues are shown in green. **(B)** Schematic of chimeric integrin α subunit. Determined functions of INA-1 and PAT-2 and the predicted outcome of INA-1/PAT-2 chimeric integrin expression in the pharynx are listed. **(C)** A merged fluorescence image of *myo-2p*::[INA-1/PAT-2]::mNG (green) and laminin::mKate2 (magenta) in a 72-h adult pharynx is shown. Laminin::mKate2 signal in the boxed region is magnified in the inset. Quantification of the fold change in pharyngeal BM laminin::mKate2 fluorescence intensity upon overexpression of the INA-1/PAT-2 chimera is shown on the right (n = 9). ***, $P < 0.0001$, paired two-tailed Student's t test. **(D)** A merged fluorescence image of *myo-2p*::[INA-1/PAT-2]::mNG (green) and collagen::mCh (magenta) in a 72-h adult pharynx is shown. Collagen::mCh signal in the boxed region is magnified in the inset. Quantification of the fold change in pharyngeal BM collagen::mCh fluorescence intensity upon overexpression of the INA-1/PAT-2 chimera is shown on the right (n = 21). n.s. (not significant), $P > 0.05$, paired two-tailed Student's t test. Box edges in boxplots depict the 25th and 75th percentiles, the line in the box indicates the median value, and whiskers mark the minimum and maximum values. Scale bars, 10 µm.

PAT-2 might function in the same genetic pathway to mediate type IV collagen recruitment, we first generated a *rap-3* null mutation, *rap-3(qy67)*, using CRISPR/Cas9 genome editing. However, we were unable to view homozygous *rap-3(qy67)* mutant larval animals due to embryonic lethality. To circumvent embryonic lethality, we knocked down *pat-2* and *rap-3* simultaneously by RNAi beginning at the L1 larval stage. The combined RNAi against *rap-3* and *pat-2* did not worsen the reduction in pharyngeal BM collagen levels caused by individual *pat-2* or *rap-3* knockdown, consistent with these genes functioning within the same pathway (Fig. S5 C). We also found that knockdown of *rap-3* did not alter PAT-2 or PAT-3 localization or levels (Fig. S5 D), suggesting that it does not activate PAT-2/PAT-3 by regulating integrin trafficking. Together, our observations support the idea that RAP-3 is a pharyngeal-specific activator of the PAT-2/PAT-3 integrin, triggering its ability to recruit type IV collagen to the pharyngeal BM.

Finally, we wanted to test if ectopic expression of RAP-3 in the gonad was sufficient to activate PAT-2/PAT-3 in this tissue to facilitate collagen recruitment. We used the *inx-8* promoter

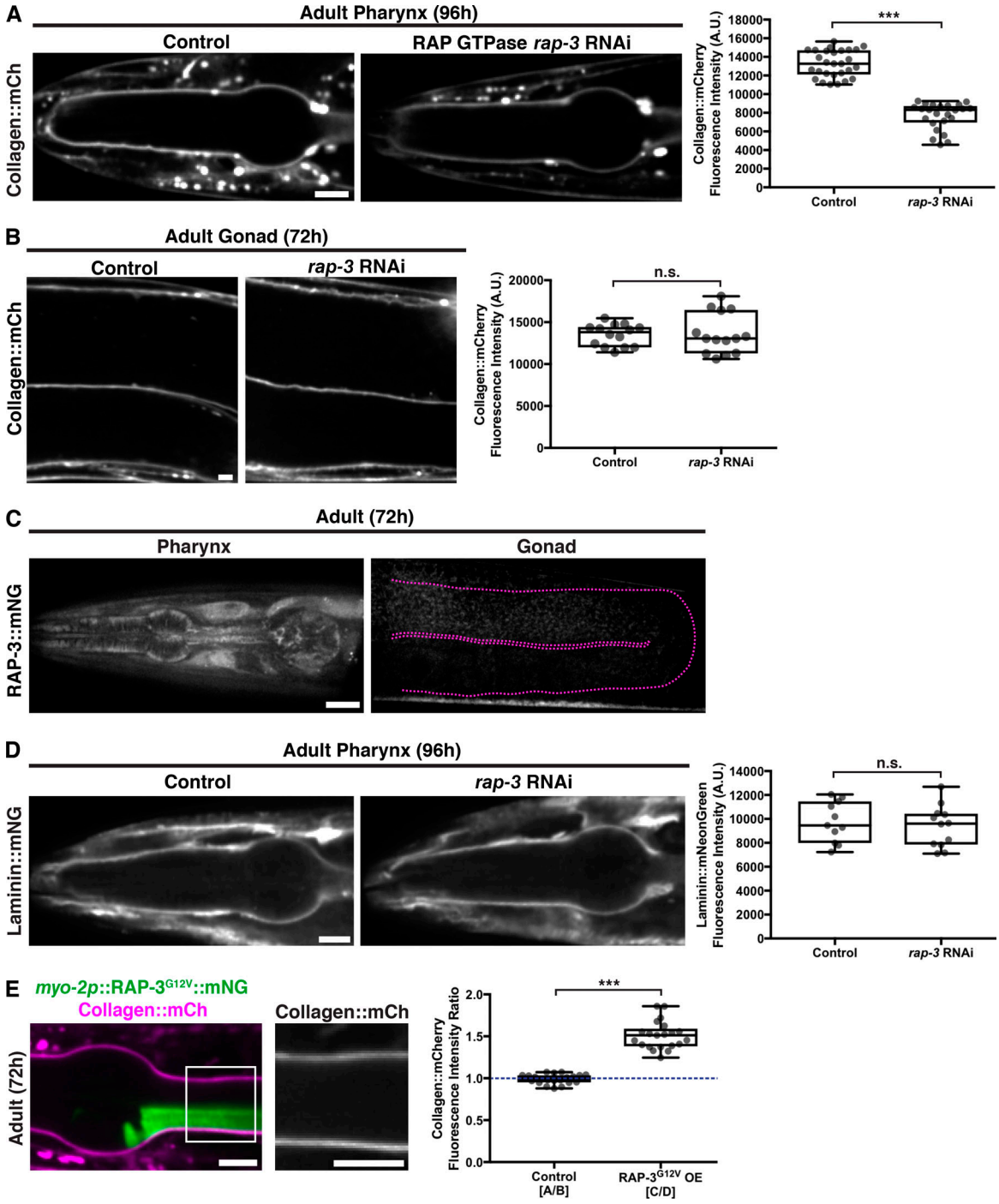

Figure 7. **RAP-3 regulates the PAT-2/PAT-3-driven recruitment of collagen into the pharyngeal BM. (A)** Fluorescence images of pharyngeal BM collagen::mCh in control and *rap-3* RNAi-treated 96-h adult animals, with quantification of collagen::mCh fluorescence intensity on the right (control, *n* = 28; *rap-3* RNAi, *n* = 24). **(B)** Fluorescence images of gonadal BM collagen::mCh in control and *rap-3* RNAi-treated 72-h adult animals, with quantification of collagen::mCh fluorescence intensity on the right (control, *n* = 14; *rap-3* RNAi, *n* = 14). **(C)** Fluorescence images of RAP-3::mNG localization in the pharynx and its absence in the gonad (outlined in magenta). **(D)** Fluorescence images of pharyngeal BM laminin::mNG in control and *rap-3* RNAi-treated 96-h adult animals, with quantification of laminin::mNG fluorescence intensity on the right (control, *n* = 11; *rap-3* RNAi, *n* = 12). ***, P < 0.0001, unpaired two-tailed Student's *t* test; n.s. (not significant), P > 0.05. **(E)** Merged fluorescence image of *myo-2p*::RAP-3^{G12V}::mNG (green) and collagen::mCh (magenta) in a 72-h adult pharynx. Pharyngeal BM collagen::mCh signal in the boxed region is magnified on the right. Quantification of fold increase in collagen::mCh fluorescence intensity upon RAP-3^{G12V} overexpression is shown on the right (*n* = 21). ***, P < 0.0001, paired two-tailed Student's *t* test. Box edges in boxplots depict the 25th and 75th percentiles, the line in the box indicates the median value, and whiskers mark the minimum and maximum values. Scale bars, 10 µm. A.U., arbitrary units.

and extrachromosomal mosaic expression to drive RAP-3::mNG expression in the gonadal sheath cells (Starich et al., 2014) that contact BM (Fig. 8 A). Strikingly, we found that ectopic mosaic RAP-3 expression in the gonadal sheath cells increased collagen levels by ∼80% in regions of the BM contacting RAP-3–expressing cells (Fig. 8 A). We predicted that if RAP-3 was triggering collagen recruitment by activating PAT-2/PAT-3 in the gonad, then laminin levels would not be altered. Consistent with this, we found that gonadal expression of RAP-3 did not affect BM laminin levels (Fig. 8 B). Together, these observations strongly suggest that RAP-3 is a tissue-specific activator of PAT-2/PAT-3 integrin, which directs the laminin-independent addition of type IV collagen into the BM.

Discussion

Type IV collagen is critical for BM function, and numerous human diseases are associated with its misregulated accumulation or loss (Fidler et al., 2018). Previous work has suggested that a meshwork of laminin forms a cell-bound template that recruits the type IV collagen network through cross-bridging components (Glentis et al., 2014; Pozzi et al., 2017). How laminin is targeted to cell surfaces and whether there are other mechanisms to direct collagen to BMs in vivo has remained unclear. Through live-cell imaging of endogenous localization, conditional knockdown, misexpression, and RNAi screening, we have discovered distinct mechanisms for type IV collagen recruitment to the growing BMs of the *C. elegans* pharyngeal and gonadal tissues. We found that the two *C. elegans* integrin α subunits, INA-1 (laminin-binding) and PAT-2 (RGD-binding), are expressed with the sole β subunit PAT-3 in both organs. Our results suggest each tissue promotes selective activation of a specific integrin heterodimer to recruit collagen from the extracellular fluid: αINA-1/βPAT-3 activation in the gonad recruits laminin, which directs moderate amounts of collagen to the BM, while αPAT-2/βPAT-3 activation in the pharynx recruits high levels of collagen in an apparently laminin-independent manner. Supporting this model, we identified a putative pharyngeal-specific PAT-2/PAT-3 activator, the small GTPase RAP-3, which is an orthologue of mammalian Rap1 that mediates inside-out activation of mammalian integrins (Boettner and Van Aelst, 2009). Collectively, these data reveal how tissues dictate collagen incorporation into BM through selective integrin activation and provide insight into how cells can use distinct mechanisms to target collagen to BMs, thereby precisely controlling collagen levels and constructing diverse BMs (Fig. 8 C).

Due to the challenge of imaging of BMs in situ, the lethal phenotypes of null mutations of many BM components, and the expanded gene families of BM receptors and matrix components in vertebrates, it has been difficult to establish the mechanisms that mediate type IV collagen recruitment to BMs in vivo (Yurchenco and Patton, 2009; Li et al., 2017). Studies in vitro have suggested that several mechanisms might recruit laminin to cell surfaces, which in turn mediates type IV collagen incorporation. For example, work on embryoid bodies—groups of pluripotent embryonic stem cells—has indicated that integrin β1 and dystroglycan matrix receptors function redundantly to promote the anchorage of laminin to the surfaces of cells (Li et al., 2017). Findings in cultured rat Schwann cells have further suggested that sulfated glycolipids mediate laminin deposition (Li et al., 2005). Here, we exploited the small BM receptor and matrix families of *C. elegans* (Clay and Sherwood, 2015), as well as their conditional knockdown by RNAi, to investigate how the sole *C. elegans* type IV collagen molecule is recruited to the BMs of growing gonadal and pharyngeal organs during larval development. We demonstrate that the two *C. elegans* integrin heterodimers play key roles in BM recruitment: αINA-1/βPAT-3 promotes laminin-dependent type IV collagen recruitment to the gonadal BM, while αPAT-2/βPAT-3 directs collagen IV to the pharyngeal BM in a manner that appears to be independent of laminin. RNAi against these integrins did not reduce type IV collagen incorporation into the BMs as severely as knockdown of type IV collagen itself, suggesting that another cell surface system may function with integrin. However, *C. elegans* does not synthesize sulfated glycolipids (Bai et al., 2018), and knockdown of neither dystroglycan nor the matrix receptors glypican, discoidin domain receptors, leukocyte common antigen-related receptor protein tyrosine phosphatase, or teneurin reduced type IV collagen recruitment. Thus, integrins are likely the chief mediators of type IV collagen recruitment to the gonadal and pharyngeal BMs.

Laminin is required for the recruitment of type IV collagen to the BM of *Drosophila* and mouse embryos (Pöschl et al., 2004; Urbano et al., 2009; Matsubayashi et al., 2017). In addition, in embryoid bodies, the inhibition of laminin polymerization prevents the assembly of collagen IV on cell surfaces (Li et al., 2002). Further, in cultured Schwann cells, exogenously added collagen assembles into the BM-like matrix only in the presence of laminin (Tsiper and Yurchenco, 2002). Similarly, we found that collagen IV targeting to the gonadal BM was dependent on laminin. Comparatively little is known about laminin-independent collagen recruitment. BM collagen addition independent of laminin has recently been observed during wound repair in the *Drosophila* larval epidermal BM (Ramos-Lewis et al., 2018), but the receptors facilitating this mode of collagen targeting have not been identified. In our study, we found that reduction of laminin did not alter type IV collagen addition to the pharyngeal BM. We discovered that the PAT-2/PAT-3 integrin is required to recruit type collagen IV to the pharyngeal BM but not laminin. Further, we found that overexpression of a chimeric α-integrin subunit in the pharynx resulted in an increase in BM laminin levels, but collagen levels were unchanged. Taken together, these observations suggest a laminin-independent mode of PAT-2/PAT-3–mediated collagen recruitment to the larval pharyngeal BM. Importantly, we cannot definitively rule out a role for laminin, as we currently lack experimental means to eliminate laminin from postembryonic BMs. Genetic loss of laminin in embryos disrupts the later addition of type IV collagen during embryogenesis, although it is unclear if this is a result of a role for laminin in type IV collagen recruitment or because of an earlier role for laminin in polarizing the pharyngeal epithelium (Rasmussen et al., 2012). One possibility during BM expansion in the larval pharynx is that a small amount of preexisting laminin matrix is sufficient to facilitate PAT-2/

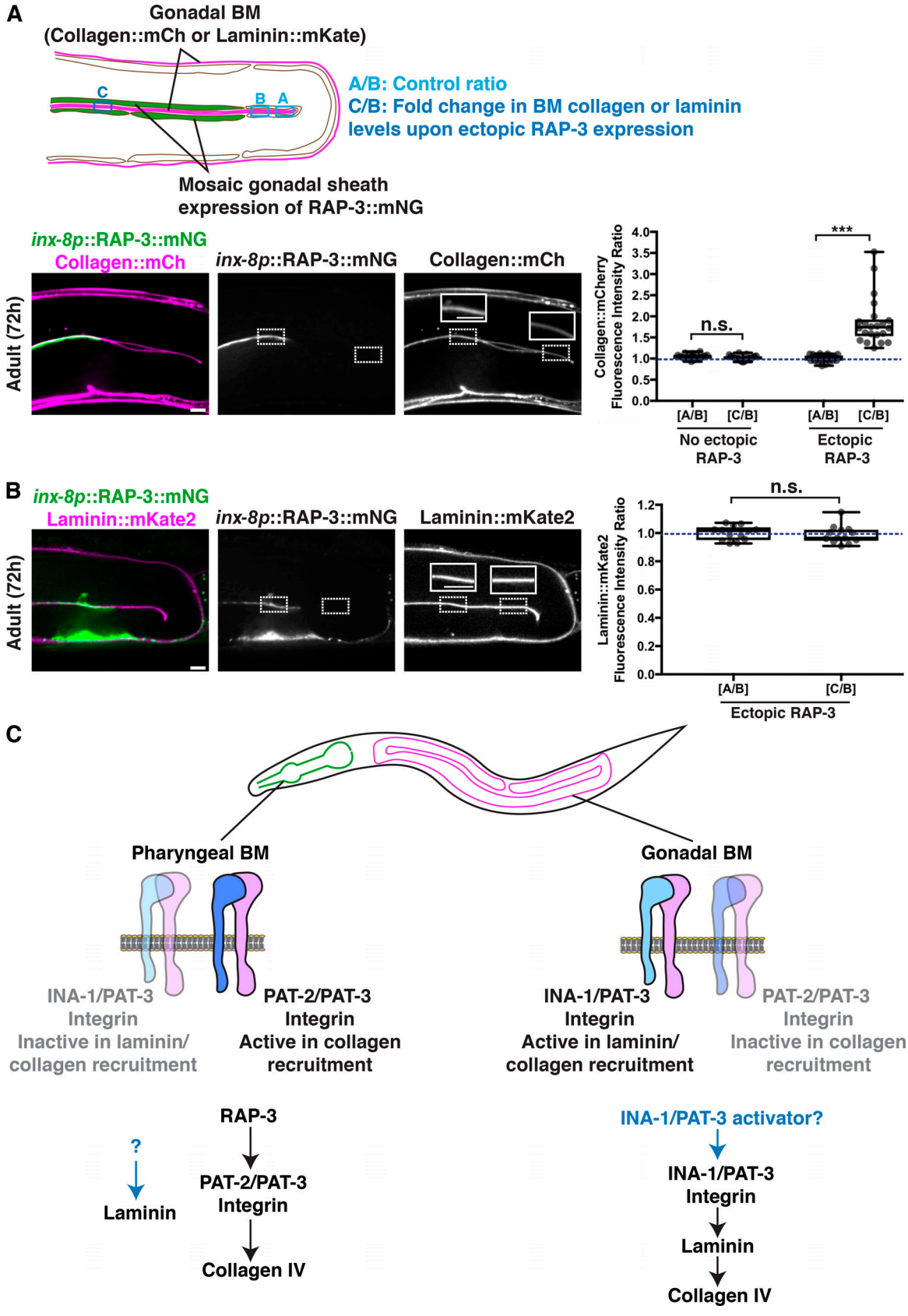

Figure 8. **Ectopic gonadal expression of RAP-3 increases BM collagen but not laminin levels. (A)** A schematic outlining mosaic expression of RAP-3::mNG in the gonadal sheath cells and method for quantification of collagen and laminin levels is shown on top. A merged fluorescence image of *inx-8p*::RAP-3::mNG (green) and collagen::mCh (magenta) in a 72-h adult gonad is shown on the bottom left, and split RAP-3::mNG and collagen::mCh channel images are shown on

the bottom right. The dotted box on the left indicates a region of RAP-3 expression, and the dotted box on the right denotes absence of RAP-3 expression. Collagen::mCh signal in the dotted box regions are magnified in insets. Quantification of fold increase in gonadal BM collagen::mCh fluorescence intensity upon ectopic RAP-3 expression is shown on the right (n = 22). **(B)** A merged fluorescence image of *inx-8p*::RAP-3::mNG (green) and laminin::mKate2 (magenta) in a 72-h adult gonad is shown on the left, and split RAP-3::mNG and laminin::mKate2 channel images on the right. The dotted box on the left indicates a region of RAP-3 expression, and the dotted box on the right denotes absence of RAP-3 expression. Laminin::mKate2 signal in the dotted box regions are magnified in insets. Quantification of fold increase in gonadal BM laminin::mKate2 fluorescence intensity upon ectopic RAP-3 expression is shown on the right (n = 13). ***, $P < 0.0001$, paired two-tailed Student's t test; n.s. (not significant), $P > 0.05$. **(C)** Model for distinct modes of collagen recruitment to the pharyngeal and gonadal BMs. Box edges in boxplots depict the 25th and 75th percentiles, the line in the box indicates the median value, and whiskers mark the minimum and maximum values. Scale bars, 10 µm.

PAT-3–mediated type IV collagen assembly. In support of this possibility, small amounts of laminin facilitate collagen assembly in cultured rat Schwann cells and cultured mouse myoblasts (McKee et al., 2009, 2017).

While BMs arose at the time of animal multicellularity, laminin- and type IV collagen–related genes and integrin receptors are present in unicellular protists that are sister groups to metazoans (King et al., 2008; Babonis and Martindale, 2017; Fidler et al., 2017; Grau-Bové et al., 2017). Thus, laminin- and type IV collagen–like proteins had roles independent of BMs and potentially independently of each other in unicellular ancestors of animals. How type IV collagen recruitment became dependent on laminin in the construction of BMs is unclear (Fidler et al., 2017). Further, it is possible that the apparently laminin-independent recruitment of collagen IV to the pharyngeal BM reflects an ancient collagen-specific targeting to cell surfaces that is used for tissue-specific BM construction. Alternatively, distinct modes of BM recruitment could be a mechanism that arose independently in animals to build unique BMs. Understanding the functions and interactions of laminin- and type IV collagen–like molecules in unicellular protists and basal metazoans will likely provide important insights into the origins of BMs and their diverse construction.

Sequence analysis suggests that PAT-2/PAT-3 is an RGD-binding integrin (Brown, 2000). As multiple RGD sequences are present in both α1 and α2 chains of *C. elegans* collagen IV, it is possible that PAT-2/PAT-3 directly binds collagen, thus precluding the need for a laminin template. Supporting this notion, we found that mosaic overexpression of PAT-2/PAT-3 in the pharyngeal tissue caused an increase in BM collagen levels only in regions of the BM contacting overexpressed PAT-2/PAT-3. Countering this idea, it has been suggested that the RGD sequences in collagen may not be sterically accessible to integrins (Khoshnoodi et al., 2008). Hence, an alternative possibility is that PAT-2/PAT-3 binds either to a cell surface or BM molecule that directly interacts with collagen. In *Drosophila*, the RGD-binding PS2 integrin (orthologous to PAT-2/PAT-3) binds to the extracellular matrix protein tiggrin, but it is unclear if tiggrin binds to type IV collagen or other matrix proteins (Fogerty et al., 1994; Bunch et al., 1998). The *C. elegans* genome does not encode tiggrin. However, one potential analogous ligand for PAT-2/PAT-3 integrin is UNC-52/perlecan, as it possesses RGD sequences and is localized to muscle attachment sites where PAT-2/PAT-3 is enriched (Gieseler et al., 2017).

Both the integrin α subunits INA-1 and PAT-2 and the β subunit PAT-3 are expressed in the gonad and the pharynx. Thus, tissue-specific integrin expression cannot account for the tissue-specific activity of gonadal INA-1/PAT-3 and pharyngeal PAT-2/PAT-3 in collagen recruitment. We considered the possibility that tissue-specific synthesis of laminin or type IV collagen might selectively activate gonadal INA-1/PAT-3 or pharyngeal PAT-2/PAT-3 heterodimers, respectively, as they are trafficked to cell surfaces (analogous to outside-in activation of integrin). However, this is unlikely, as laminin is produced by both tissues (Huang et al., 2003) and collagen is not synthesized in the pharyngeal epithelium (Graham et al., 1997). Since the sole difference between the αINA-1/βPAT-3 and the αPAT-2/βPAT-3 integrins is the α subunit, we propose instead that tissue-specific factors activate αINA-1 or αPAT-2 to promote their tissue-specific matrix-recruiting activity. One possible mode of activation is through the diverse cytoplasmic tail region of the α subunits. Studies in mammalian cell lines have shown that the cytoplasmic tails of α-integrin subunits are required for the inside-out activation of integrin receptors and may bestow specificity to integrin activation (Liu et al., 2015; Thinn et al., 2018). Supporting this idea, we found that expressing the PAT-2 α-integrin cytoplasmic tail fused to the INA-1 extracellular domain in the pharynx activated its ability to recruit laminin, even though INA-1 does not normally function in pharyngeal BM laminin recruitment during larval development. One puzzling question is the functional significance of the α subunit expressed in each tissue and localized to the cell–BM interface but not involved in BM recruitment. In the gonad, our evidence suggests that the α subunit PAT-2 acts in part to sequester the β subunit PAT-3, thus limiting the amount of active INA-1/PAT-3 heterodimer and thereby limiting laminin addition to the BM. It is also possible that α subunits not involved with BM recruitment may help localize proteases involved in matrix remodeling (Desgrosellier and Cheresh, 2010) or might be associated with intracellular effectors that allow it to be activated and signal in response to changing matrix and physiological conditions (Wolfenson et al., 2013).

In lymphocytes, coexpressed integrins αLβ2 and αMβ2, which share a common β subunit, are differentially activated through their divergent α cytoplasmic tails, triggering distinct adhesion responses to chemokine stimulation (Weber et al., 1999). Notably, the mammalian small GTPase Rap1 facilitates the activation of the αLβ2-integrin through the lymphoid-enriched Rap1 effector molecule RapL, which binds to the αL subunit (Katagiri et al., 2004; Zhang and Wang, 2012). In our study, through a targeted RNAi screen, we identified RAP-3, a *C. elegans* orthologue of mammalian Rap1, as a pharyngeal-expressed activator of the PAT-2/PAT-3 integrin's collagen IV recruiting function. *C. elegans* encodes two Rap1 orthologues,

rap-1 and *rap-3* (Reiner and Lundquist, 2018), with *rap-3* appearing to be more divergent (Rasmussen et al., 2018). We provide strong evidence that RAP-3 is a specific activator of PAT-2/PAT-3 integrin. First, similar to loss of PAT-2/PAT-3, loss of RAP-3 resulted in reduction of pharyngeal BM collagen but not laminin levels. Second, overexpression of a constitutively active mutant of RAP-3 in the pharyngeal epithelium increased collagen levels in regions of the pharyngeal BM contacting overexpressing cells, phenocopying our observations with pharyngeal PAT-2 overexpression. Third, our genetic analysis suggested that RAP-3 and PAT-2 act in the same pathway to promote collagen recruitment. Finally, ectopic expression of RAP-3 in the gonad increased type IV collagen levels in the gonadal BM, but not laminin levels, indicative of ectopic PAT-2/PAT3 activation. The effectors of RAP-3 that promote PAT-2/PAT-3 activity in collagen recruitment to the BM are not known, but our data suggest they are likely expressed in both gonadal and pharyngeal tissues, as RAP-3 can activate PAT-2/PAT-3 in either tissue. Collectively, these observations support a model where the tissue-specific expression of RAP-3 in the pharynx promotes activation of PAT-2/PAT-3 to facilitate laminin-independent collagen recruitment to the BM and suggest that distinct tissue-specific factors might mediate INA-1/PAT-3 activation in the gonad to promote laminin-dependent BM collagen recruitment (Fig. 8 C).

The triple-helical nature of collagen combined with its intermolecular covalent cross-links provides BMs their tensile strength, and genetic elimination of type IV collagen results in embryonic lethality in mice and *C. elegans* when tissues first experience mechanical loads (Gupta et al., 1997; Pöschl et al., 2004). Type IV collagen also tethers numerous matrix proteins and growth factors (Fidler et al., 2018). As a result of its complex and essential roles, precise levels of BM collagen are required for many cell and tissue functions. For example, the bone morphogenetic protein/TGFβ ligand Dpp binds type IV collagen in *Drosophila* BMs, and collagen levels influence Dpp-mediated signaling during dorsal ventral patterning in the embryo, germ stem cell production in the ovary, renal tubule morphogenesis, and wing disc growth (Wang et al., 2008; Bunt et al., 2010; Ma et al., 2017). Further, specific levels and gradients of type IV collagen mediate tissue constriction and shaping in the *Drosophila* egg chamber and wing disc and the *C. elegans* gonad (Kubota et al., 2012; Morrissey and Sherwood, 2015; Crest et al., 2017). Distinct integrin receptors that mediate different modes of type IV collagen recruitment may provide tissues with robust mechanisms to control BM collagen levels. In particular, as PAT-2/PAT3 activity is controlled by the small GTPase RAP-3, its activity, and thus levels of type IV collagen, can be finely tuned through GTPase-activating proteins and guanine nucleotide exchange factors. This could be a dynamic mechanism for tissues to increase, decrease, and even translate signaling pathways into collagen gradients (Crest et al., 2017; Jayadev and Sherwood, 2017). Therapeutically targeting specific activators of collagen-recruiting integrins may also be a promising means to modulate collagen levels during aging, in fibrotic diseases, and with type IV collagen genetic disorders where type IV collagen levels in BMs are altered, leading to tissue decline (Uspenskaia et al., 2004; Mao et al., 2015; Karsdal et al., 2016; Fidler et al., 2018).

Materials and methods

C. elegans strains

C. elegans strains used in this study are listed in Table S2. Worms were reared on nematode growth medium plates seeded with OP50 *Escherichia coli* at 16°C, 18°C, or 20°C according to standard procedures (Stiernagle, 2006).

Transgene construction

mNG/mKate2 knock-ins

To generate the following functional, genome-edited mNG knock-ins *lam-2(qy20[lam-2::mNG + LoxP])*, *lam-2(qy41[lam-2::mKate2 + LoxP])*, *pat-3(qy36[pat-3::mNG + LoxP])*, *ina-1(qy23[ina-1::mNG + LoxP])*, *pat-2(qy26[pat-2::mNG + LoxP])*, *pat-2(qy49[pat-2::2xmNG + LoxP])*, and *rap-3(qy57[rap-3::mNG + LoxP])*, we used CRISPR/Cas9 genome editing with a self-excising cassette (SEC) for drug (hygromycin) selection as described previously (Dickinson et al., 2015), with some modifications. Briefly, we generated new starter repair plasmids lacking the 3xFlag tag downstream of the SEC cassette sequence, and we attached an 18–amino acid (glycine-alanine-serine) flexible linker (flexlink) in-frame and directly upstream of mNG, mKate2, or two tandem mNG fluorophores. Approximately 700-bp to 1-kb left and right homology arms for each target were amplified from N2 genomic DNA (gDNA), mutated to introduce six silent point mutations adjacent to the Cas9 cut site, and inserted into the appropriate repair plasmid using Gibson assembly. We generated one or two single guide RNA (sgRNA) plasmids for each target by inserting the respective sgRNA sequences into the pDD122 plasmid. To direct cleavage near the C-terminus, the following sgRNA sequences were used: 5′-GTCATCAATTTGGAGCAAGA-3′ and 5′-ATTGATGACATTGAAGCATT-3′ for *lam-2*; 5′-TTGGCTTTTCCAGCGTATAC-3′ and 5′-TTTAAAAATCCAGTATACGC-3′ for *pat-3*; 5′-CGAGAAGAATGGGCTGATAC-3′ and 5′-ACGAGAAGAATGGGCTGATA-3′) for *ina-1*; and 5′-CAGTACAATCAGGGACGTCA-3′ for *pat-2*; and 5′-ATCTAATCGTGTGCAAAACA-3′ for *rap-3*. For each tagging experiment, we injected a mixture of 50 ng/µl Cas9-sgRNA plasmids (25 ng/µl of each guide plasmid in cases where two sgRNAs were available), 100 ng/µl repair template plasmid, and red coinjection markers (2.5 ng/µl pCFJ90 [*myo-2p::mCherry*] and 5 ng/µl pCFJ104 [*myo-3p::mCherry*]) into the gonads of ∼30–40 young adult N2 animals. The injected animals were singled onto fresh OP50 plates and allowed to lay eggs for 3–4 d at 20°C in the absence of selection. Then, 500 µl of 2 mg/ml hygromycin solution was added to each plate, and the plates were returned to 20°C for 4–5 d. Candidate knock-in animals were roller (*sqt-1(e1350)*, dominant Rol mutation) worms that survived the hygromycin treatment and lacked the red fluorescent extrachromosomal array markers. We were able to isolate approximately two to five independent lines for each construct. All initial insertion strains were homozygous viable and segregated 100% Rol progeny. To excise the SEC, we heat-shocked plates containing approximately six L3/L4 rollers each at 34°C in a water bath for 4 h, and then grew the animals at 20°C for 3–4 d.

We singled adult wild-type animals (worms that lost both copies of the SEC) and verified successful genome editing by visualizing mNG/mKate2 fluorescence, PCR genotyping, and sequencing of the fluorophore insertion site.

rap-3 knockout

To generate *rap-3(qy67[mNG + SEC])*, we used CRISPR/Cas9 genome editing with the SEC as described above to delete the endogenous *rap-3* coding sequence and replace it with mNG. We directed cleavage near the N- and C-terminus of *rap-3* using the following sgRNAs: 5′-TTTTGGGAAATGGAGGAGTT-3′ and 5′-ATCTAATCGTGTGCAAAACA-3′. We modified the starter repair template plasmid described above to include 1-kb left and right homology arms for *rap-3*.

myo-2p::pat-2::mNG::unc-54 3′ UTR

myo-2p::pat-2::mNG::unc-54 3′utr was built by Gibson assembling the following fragments in order: an ∼1-kb *myo-2p* fragment from the pCFJ90 vector, full-length *pat-2* amplified from N2 gDNA, and *flexlink::mNG::unc-54 3′utr*.

myo-2p::ina-1[EX]::pat-2[CTMD]::mNG::unc-54 3′ UTR

To generate *myo-2p::ina-1[EX]::pat-2[CTMD]::mNG::unc-54 3′utr*, we first amplified full-length *ina-1* and *pat-2* from N2 gDNA and cloned these fragments into separate TOPO vectors. Then we used Gibson assembly to ligate the following fragments in order: an ∼1-kb *myo-2p* fragment from the pCFJ90 vector; *ina-1* fragment containing only the extracellular, transmembrane, and intracellular membrane-proximal regions; *pat-2* fragment containing only the CTMD; and *flexlink::mNG::unc-54 3′utr*.

myo-2p::rap-3^{G12V}::mNG::unc-54 3′ UTR

To construct *myo-2p::rap-3^{G12V}::mNG::unc-54 3′utr*, we first used Gibson assembly to connect the following fragments in order: an ∼1-kb *myo-2p* fragment from the pCFJ90 vector, full-length *rap-3* amplified from N2 gDNA, and *flexlink::mNG::unc-54 3′utr*. We then introduced the G12V mutation in *rap-3* by site-directed mutagenesis.

inx-8p::rap-3::mNG::unc-54 3′ UTR

To build *inx-8p::rap-3::mNG::unc-54 3′utr*, we replaced (by Gibson assembly) the *myo-2p* fragment in the *myo-2p::rap-3::mNG::unc-54 3′utr* construct created above with a 1.5-kb fragment upstream of *inx-8* amplified from N2 gDNA.

Transgenic strains

All CRISPR/Cas9 genome-edited mNG/mKate2 knock-in strains were created by injecting the relevant constructs into the germline of young adult N2 worms as described earlier. All knock-in alleles were functional, and viability and growth rates of knock-in strains were similar to those of N2 animals. The *rap-3(qy67)* knockout strain was generated by injecting the relevant CRISPR/Cas9 constructs into the gonads of young adult NK364 animals. We were unable to isolate homozygous *rap-3(qy67)* animals, as the null mutation caused embryonic lethality.

Transgenic worms expressing *myo-2p::pat-2::mNG::unc-54 3′utr* or *myo-2p::ina-1[EX]::pat-2[CTMD]::mNG::unc-54 3′utr* were created by injecting these constructs (1.5 ng/µl) together with full-length *pat-3* gDNA amplified from N2, EcoRI-digested salmon sperm DNA (50 ng/µl), and pBluescript II (50 ng/µl) into the gonads of young adult NK364 or NK2446 animals, respectively. Animals expressing *myo-2p::rap-3^{G12V}::mNG::unc-54 3′utr* were created by coinjecting the construct (1.5 ng/µl) with EcoRI-digested salmon sperm DNA (50 ng/µl) and pBluescript II (50 ng/µl) into the gonads of young adult NK364 animals. Worms carrying *inx-8p::rap-3::mNG::unc-54 3′utr* were made by coinjecting the construct (50 ng/µl), EcoRI-digested salmon sperm DNA (50 ng/µl), pBluescript II (50 ng/µl), and a green coinjection marker (*myo-2p::gfp*, 2.5 ng/µl) into the gonads of NK364 or NK2446 animals. All of the above constructs were expressed mosaically in tissues as extrachromosomal arrays (Yochem and Herman, 2003). As the F1 progeny did not transmit these arrays stably to F2 progeny, we collected and imaged mosaic expression in F1s directly for the relevant experiments.

RNAi

All RNAi constructs were obtained from the Vidal (Rual et al., 2004) and Ahringer (Kamath et al., 2003) libraries, except for the following clones: *csk-1*, *kin-32*, *pix-1*, *rsu-1*, *unc-97*, *unc-112*, and *pat-3*. To build these RNAi clones, we PCR-amplified fragments corresponding to the longest transcripts of these genes from N2 gDNA and inserted them into the L4440 (pPD129.36) vector (Timmons and Fire, 1998) by Gibson assembly. The forward and reverse primers used to amplify these fragments are as follows: *csk-1*, 5′-TGAGCAACGGGAACAGCTACAA-3′ and 5′-CACCATAAACTTGGCTTCATCCA-3′; *kin-32*, 5′-CAAAGGCGCTGACCATCATCTA-3′ and 5′-CCGCGTAAATCTGATCAACAGTT-3′; *pix-1*, 5′-ACAAACTCCAGCGATCTCGATCC-3′ and 5′-CCCATCGTTAGAGTGAATTCTCC-3′; *rsu-1*, 5′-GAGGTTGAGCATGTCGATCGGA-3′ and 5′-CGGCTTGTTGAATTCCTTTTC-3′; *unc-97*, 5′-TGGTGTGTGGCGGAATGGATTCC-3′ and 5′-CTTTTGGTCCAGGACTCATCGAT-3′; *unc-112*, 5′-ATGTTGAACGAGATTGGTCTGAT-3′ and 5′-CCTTGAGATGTCGAATTTCCCAG-3′; *pat-3*, 5′-ATGCCACCTTCAACATCATTGC-3′ and 5′-CATTACAAGCCAACGCCTGAACA-3′. RNAi constructs were then transformed into *E. coli* strain HT115, and all RNAi experiments were performed using the feeding method (Timmons et al., 2001). Briefly, we grew RNAi bacterial cultures in selective media for 12–14 h at 37°C, and then for an additional hour following addition of 1 mM IPTG to induce double-strand RNA expression. For codepletion experiments, we mixed the relevant induced bacterial cultures at a 1:1 ratio. Nematode growth medium agar plates containing topically applied 1-M IPTG and 100-mg/ml ampicillin (9 µl each) were then seeded with these RNAi bacterial cultures and left at room temperature overnight for further induction. Synchronized L1 worms were placed on RNAi plates and allowed to feed for 24–96 h at 20°C, depending on the experiment. The L4440 empty vector was used as a negative control for all RNAi experiments. To improve RNAi knockdown efficiency in the pharyngeal tissue, we used worms harboring the *lin-35(n745)* mutant allele (Shiu and Hunter, 2017), and to enhance sensitivity to RNAi in the gonadal sheath and other tissues, we used the *rrf-3(pk1426)* genetic background (Simmer et al., 2002). We verified knockdown efficiency for all RNAi experiments, with

the exception of the targeted RNAi screen and *pat-2; pat-3* double RNAi experiments, by including a control with the relevant mNG/mCherry/mKate2-tagged target protein. We achieved between ∼70 and 100% reduction for all RNAi experiments. For the codepletion of PAT-2 and RAP-3, we verified knockdown efficiency by plate-level assessment of worm paralysis: RNAi initiated at the L1 larval stage against *pat-2* alone, or *pat-2* and *rap-3* in combination, resulted in 100% paralysis of animals by early adulthood.

Imaging

Confocal differential interference contrast (DIC) and fluorescence images were acquired at 20°C on an AxioImager A1 microscope (Carl Zeiss) controlled by µManager software (Edelstein et al., 2010) and equipped with an electron-multiplying charge-coupled device camera (Hamamatsu Photonics), a 40× Plan-Apochromat (1.4-NA) objective, a spinning disc confocal scan head (CSU-10; Yokogawa Electric Corp.), and 488- and 561-nm laser lines. Worms were mounted on 5% noble agar pads containing 0.01 M sodium azide for imaging. For all experiments except those detailed in Figs. 1 B and S3 A, we captured single-slice images at the middle focal plane of animals where most or all of the gonadal and pharyngeal tissue cross sections were in focus. For Fig. 1 B, we acquired z-stacks at 1-µm intervals spanning the entirety of the pharynx or gonad. For Fig. S3 A, we captured single-slice images at a superficial focal plane, where the body wall muscle was in focus.

Image analysis, processing, and quantification

All quantifications of mean fluorescence intensity were done on raw images in Fiji 2.0 (Schindelin et al., 2012). We drew ∼5–8-pixel-long linescans along the BM to obtain raw values of mean fluorescence intensity. Background intensity values were obtained by averaging two linescans of similar length in regions adjacent to the BM with no visible fluorescence signal. DIC and fluorescence images in all figures were processed in Fiji. The unsharp mask filter was applied to DIC images. 3D isosurface renderings of the pharyngeal and gonadal BMs were constructed using Imaris 7.4 software (Bitplane). Briefly, we acquired z-stacks of pharyngeal and gonadal collagen::mCh in early L1 and young adult worms. Young adult gonads were imaged in sections, and z-stacks of individual sections were stitched together with the Fiji pairwise stitching method (Preibisch et al., 2009). 3D isosurfaces were constructed from these z-stacks by manually tracing the outline of BM collagen::mCh in every z-slice, and surface area measurements were automatically calculated from these isosurfaces by Imaris.

Statistical analysis

Statistical analysis was performed in GraphPad Prism 7. To blind analysis of fluorescence intensity in all datasets, we used a filename-randomizing macro (courtesy of Martin Höhne, University of Cologne, Cologne, Germany) in ImageJ (National Institutes of Health). Sample sizes were validated a posteriori through assessments of normality by log-transforming all datasets and then using the Shapiro–Wilk test. For comparisons of mean fluorescence intensities between two populations, we used an unpaired two-tailed Student's *t* test (with Welch's correction in cases of unequal variance between samples). To compare mean fluorescence intensities between three or more populations, we performed one-way ANOVA followed by either a post hoc Dunnett's or Tukey's multiple comparison test. For comparisons of fluorescence intensity ratios, we used a paired two-tailed Student's *t* test (with Welch's correction in cases of unequal variance between samples). Bar graphs and boxplots were prepared in GraphPad Prism 7. Figure legends indicate sample sizes, statistical tests used, and P values.

Online supplemental material

Fig. S1, related to Fig. 3, shows the quantification of pharyngeal and gonadal BM laminin levels upon *lam-2* knockdown. Fig. S2 shows DGN-1::mNG localization at the gonadal sheath–BM interface, *dgn-1* knockdown efficiency, and quantification of gonadal BM laminin and collagen levels upon reduction of DGN-1. Fig. S3, related to Fig. 4, shows integrin subunit knockdown efficiency, muscle collagen levels upon integrin knockdown, gonadal BM INA-1::mNG levels upon reduction of PAT-2, and quantification of gonadal collagen levels upon knockdown of various matrix receptors. Fig. S4, related to Fig. 5, shows DGN-1::mNG localization in the head of the worm, integrin subunit knockdown efficiency, and quantification of pharyngeal BM collagen levels upon reduction of matrix receptors. Fig. S5, related to Fig. 7, shows RAP-3::mNG localization in the L1 larva, *rap-3* knockdown efficiency, collagen levels upon codepletion of PAT-2 and RAP-3, and PAT-2::mNG and PAT-3::mNG levels upon *rap-3* knockdown. Table S1, related to Fig. 7, describes the targeted screen of integrin-associated proteins. Table S2 lists *C. elegans* strains used in this study.

Acknowledgments

We thank Brent Hoffman, Kacy Gordon, David Reiner, Arnoud Sonnenberg, Thomas Hannich, Nick Brown, Roy Zent, and members of the Sherwood laboratory for helpful discussions.

Some strains were provided by the Caenorhabditis Genetics Center, which is funded by National Institutes of Health Office of Research Infrastructure Programs (P40 OD010440). E.L. Hastie was supported by American Cancer Society postdoctoral fellowship 129351-PF-16-024-01-CSM, and D.R. Sherwood was supported by the National Institute of General Medical Sciences (Maximizing Investor's Research Award R35 GM118049), and the National Institute of Child Health and Human Development (R21 HD084290).

The authors declare no competing financial interests.

Author contributions: R. Jayadev and D.R. Sherwood conceived the project. R. Jayadev designed and performed all experiments and analyzed and interpreted the data, with the following contributions from other authors. Q. Chi designed and built molecular biology constructs used in Figs. 2; 4 A; 7, C and E; and 8 and Table S1; D.P. Keeley acquired and analyzed the data on gonadal growth (Fig. 1 B); E.L. Hastie and D.P. Keeley generated the endogenously tagged integrin subunit strains; and L.C. Kelley conceived the integrin chimera experiment (Fig. 6 A).

R. Jayadev prepared the figures. R. Jayadev and D.R. Sherwood wrote the manuscript.

Submitted: 20 March 2019
Revised: 16 June 2019
Accepted: 10 July 2019

References

Babonis, L.S., and M.Q. Martindale. 2017. Phylogenetic evidence for the modular evolution of metazoan signalling pathways. *Philos. Trans. R. Soc. Lond. B Biol. Sci.* 372:20150477. https://doi.org/10.1098/rstb.2015.0477

Bai, M., R. Vozdek, A. Hnízda, C. Jiang, B. Wang, L. Kuchar, T. Li, Y. Zhang, C. Wood, L. Feng, et al. 2018. Conserved roles of C. elegans and human MANFs in sulfatide binding and cytoprotection. *Nat. Commun.* 9:897. https://doi.org/10.1038/s41467-018-03355-0

Boettner, B., and L. Van Aelst. 2009. Control of cell adhesion dynamics by Rap1 signaling. *Curr. Opin. Cell Biol.* 21:684–693. https://doi.org/10.1016/j.ceb.2009.06.004

Bouvard, D., J. Pouwels, N. De Franceschi, and J. Ivaska. 2013. Integrin inactivators: balancing cellular functions in vitro and in vivo. *Nat. Rev. Mol. Cell Biol.* 14:430–442. https://doi.org/10.1038/nrm3599

Breitkreutz, D., I. Koxholt, K. Thiemann, and R. Nischt. 2013. Skin basement membrane: the foundation of epidermal integrity--BM functions and diverse roles of bridging molecules nidogen and perlecan. *BioMed Res. Int.* 2013:179784. https://doi.org/10.1155/2013/179784

Brown, N.H. 2000. Cell-cell adhesion via the ECM: integrin genetics in fly and worm. *Matrix Biol.* 19:191–201. https://doi.org/10.1016/S0945-053X(00)00064-0

Brown, K.L., C.F. Cummings, R.M. Vanacore, and B.G. Hudson. 2017. Building collagen IV smart scaffolds on the outside of cells. *Protein Sci.* 26:2151–2161. https://doi.org/10.1002/pro.3283

Bunch, T.A., M.W. Graner, L.I. Fessler, J.H. Fessler, K.D. Schneider, A. Kerschen, L.P. Choy, B.W. Burgess, and D.L. Brower. 1998. The PS2 integrin ligand tiggrin is required for proper muscle function in Drosophila. *Development.* 125:1679–1689.

Bunt, S., C. Hooley, N. Hu, C. Scahill, H. Weavers, and H. Skaer. 2010. Hemocyte-secreted type IV collagen enhances BMP signaling to guide renal tubule morphogenesis in Drosophila. *Dev. Cell.* 19:296–306. https://doi.org/10.1016/j.devcel.2010.07.019

Carmona, G., S. Göttig, A. Orlandi, J. Scheele, T. Bäuerle, M. Jugold, F. Kiessling, R. Henschler, A.M. Zeiher, S. Dimmeler, and E. Chavakis. 2009. Role of the small GTPase Rap1 for integrin activity regulation in endothelial cells and angiogenesis. *Blood.* 113:488–497. https://doi.org/10.1182/blood-2008-02-138438

Clay, M.R., and D.R. Sherwood. 2015. Basement Membranes in the Worm: A Dynamic Scaffolding that Instructs Cellular Behaviors and Shapes Tissues. *Curr. Top. Membr.* 76:337–371. https://doi.org/10.1016/bs.ctm.2015.08.001

Crest, J., A. Diz-Muñoz, D.-Y. Chen, D.A. Fletcher, and D. Bilder. 2017. Organ sculpting by patterned extracellular matrix stiffness. *eLife.* 6:e24958. https://doi.org/10.7554/eLife.24958

Desgrosellier, J.S., and D.A. Cheresh. 2010. Integrins in cancer: biological implications and therapeutic opportunities. *Nat. Rev. Cancer.* 10:9–22. https://doi.org/10.1038/nrc2748

Dickinson, D.J., A.M. Pani, J.K. Heppert, C.D. Higgins, and B. Goldstein. 2015. Streamlined Genome Engineering with a Self-Excising Drug Selection Cassette. *Genetics.* 200:1035–1049. https://doi.org/10.1534/genetics.115.178335

Edelstein, A., N. Amodaj, K. Hoover, R. Vale, and N. Stuurman. 2010. Computer control of microscopes using μManager. *Curr. Protoc. Mol. Biol.* Chapter 14:Unit14.20. https://doi.org/10.1002/0471142727.mb1420s92

Fidler, A.L., C.E. Darris, S.V. Chetyrkin, V.K. Pedchenko, S.P. Boudko, K.L. Brown, W. Gray Jerome, J.K. Hudson, A. Rokas, and B.G. Hudson. 2017. Collagen IV and basement membrane at the evolutionary dawn of metazoan tissues. *eLife.* 6:e24176. https://doi.org/10.7554/eLife.24176

Fidler, A.L., S.P. Boudko, A. Rokas, and B.G. Hudson. 2018. The triple helix of collagens - an ancient protein structure that enabled animal multicellularity and tissue evolution. *J. Cell Sci.* 131:jcs203950. https://doi.org/10.1242/jcs.203950

Fogerty, F.J., L.I. Fessler, T.A. Bunch, Y. Yaron, C.G. Parker, R.E. Nelson, D.L. Brower, D. Gullberg, and J.H. Fessler. 1994. Tiggrin, a novel Drosophila extracellular matrix protein that functions as a ligand for Drosophila alpha PS2 beta PS integrins. *Development.* 120:1747–1758.

Gieseler, K., H. Qadota, and G.M. Benian. 2017. Development, structure, and maintenance of C. elegans body wall muscle. *WormBook.* 2017:1–59. https://doi.org/10.1895/wormbook.1.81.2

Glentis, A., V. Gurchenkov, and D. Matic Vignjevic. 2014. Assembly, heterogeneity, and breaching of the basement membranes. *Cell Adhes. Migr.* 8:236–245. https://doi.org/10.4161/cam.28733

Graham, P.L., J.J. Johnson, S. Wang, M.H. Sibley, M.C. Gupta, and J.M. Kramer. 1997. Type IV collagen is detectable in most, but not all, basement membranes of Caenorhabditis elegans and assembles on tissues that do not express it. *J. Cell Biol.* 137:1171–1183. https://doi.org/10.1083/jcb.137.5.1171

Grau-Bové, X., G. Torruella, S. Donachie, H. Suga, G. Leonard, T.A. Richards, and I. Ruiz-Trillo. 2017. Dynamics of genomic innovation in the unicellular ancestry of animals. *eLife.* 6:e26036. https://doi.org/10.7554/eLife.26036

Gupta, M.C., P.L. Graham, and J.M. Kramer. 1997. Characterization of alpha1(IV) collagen mutations in Caenorhabditis elegans and the effects of alpha1 and alpha2(IV) mutations on type IV collagen distribution. *J. Cell Biol.* 137:1185–1196. https://doi.org/10.1083/jcb.137.5.1185

Hagedorn, E.J., H. Yashiro, J.W. Ziel, S. Ihara, Z. Wang, and D.R. Sherwood. 2009. Integrin acts upstream of netrin signaling to regulate formation of the anchor cell's invasive membrane in C. elegans. *Dev. Cell.* 17:187–198. https://doi.org/10.1016/j.devcel.2009.06.006

Halfter, W., P. Oertle, C.A. Monnier, L. Camenzind, M. Reyes-Lua, H. Hu, J. Candiello, A. Labilloy, M. Balasubramani, P.B. Henrich, and M. Plodinec. 2015. New concepts in basement membrane biology. *FEBS J.* 282:4466–4479. https://doi.org/10.1111/febs.13495

Harunaga, J.S., A.D. Doyle, and K.M. Yamada. 2014. Local and global dynamics of the basement membrane during branching morphogenesis require protease activity and actomyosin contractility. *Dev. Biol.* 394:197–205. https://doi.org/10.1016/j.ydbio.2014.08.014

Horton, E.R., A. Byron, J.A. Askari, D.H.J. Ng, A. Millon-Frémillon, J. Robertson, E.J. Koper, N.R. Paul, S. Warwood, D. Knight, et al. 2015. Definition of a consensus integrin adhesome and its dynamics during adhesion complex assembly and disassembly. *Nat. Cell Biol.* 17:1577–1587. https://doi.org/10.1038/ncb3257

Horton, E.R., J.D. Humphries, J. James, M.C. Jones, J.A. Askari, and M.J. Humphries. 2016. The integrin adhesome network at a glance. *J. Cell Sci.* 129:4159–4163. https://doi.org/10.1242/jcs.192054

Huang, C.-C., D.H. Hall, E.M. Hedgecock, G. Kao, V. Karantza, B.E. Vogel, H. Hutter, A.D. Chisholm, P.D. Yurchenco, and W.G. Wadsworth. 2003. Laminin alpha subunits and their role in C. elegans development. *Development.* 130:3343–3358. https://doi.org/10.1242/dev.00481

Ihara, S., E.J. Hagedorn, M.A. Morrissey, Q. Chi, F. Motegi, J.M. Kramer, and D.R. Sherwood. 2011. Basement membrane sliding and targeted adhesion remodels tissue boundaries during uterine-vulval attachment in Caenorhabditis elegans. *Nat. Cell Biol.* 13:641–651. https://doi.org/10.1038/ncb2233

Isabella, A.J., and S. Horne-Badovinac. 2015. Building from the Ground up: Basement Membranes in Drosophila Development. *Curr. Top. Membr.* 76:305–336. https://doi.org/10.1016/bs.ctm.2015.07.001

Isabella, A.J., and S. Horne-Badovinac. 2016. Rab10-Mediated Secretion Synergizes with Tissue Movement to Build a Polarized Basement Membrane Architecture for Organ Morphogenesis. *Dev. Cell.* 38:47–60. https://doi.org/10.1016/j.devcel.2016.06.009

Jayadev, R., and D.R. Sherwood. 2017. Basement membranes. *Curr. Biol.* 27:R207–R211. https://doi.org/10.1016/j.cub.2017.02.006

Jeon, T.J., D.-J. Lee, S. Merlot, G. Weeks, and R.A. Firtel. 2007. Rap1 controls cell adhesion and cell motility through the regulation of myosin II. *J. Cell Biol.* 176:1021–1033. https://doi.org/10.1083/jcb.200607072

Johnson, R.P., S.H. Kang, and J.M. Kramer. 2006. C. elegans dystroglycan DGN-1 functions in epithelia and neurons, but not muscle, and independently of dystrophin. *Development.* 133:1911–1921. https://doi.org/10.1242/dev.02363

Kamath, R.S., A.G. Fraser, Y. Dong, G. Poulin, R. Durbin, M. Gotta, A. Kanapin, N. Le Bot, S. Moreno, M. Sohrmann, et al. 2003. Systematic functional analysis of the Caenorhabditis elegans genome using RNAi. *Nature.* 421:231–237. https://doi.org/10.1038/nature01278

Karsdal, M.A., F. Genovese, E.A. Madsen, T. Manon-Jensen, and D. Schuppan. 2016. Collagen and tissue turnover as a function of age: Implications for fibrosis. *J. Hepatol.* 64:103–109. https://doi.org/10.1016/j.jhep.2015.08.014

Katagiri, K., N. Ohnishi, K. Kabashima, T. Iyoda, N. Takeda, Y. Shinkai, K. Inaba, and T. Kinashi. 2004. Crucial functions of the Rap1 effector

molecule RAPL in lymphocyte and dendritic cell trafficking. *Nat. Immunol.* 5:1045–1051. https://doi.org/10.1038/ni1111

Kedinger, M., O. Lefebvre, I. Duluc, J.N. Freund, and P. Simon-Assmann. 1998. Cellular and molecular partners involved in gut morphogenesis and differentiation. *Philos. Trans. R. Soc. Lond. B Biol. Sci.* 353:847–856. https://doi.org/10.1098/rstb.1998.0249

Kelley, L.C., L.L. Lohmer, E.J. Hagedorn, and D.R. Sherwood. 2014. Traversing the basement membrane in vivo: a diversity of strategies. *J. Cell Biol.* 204:291–302. https://doi.org/10.1083/jcb.201311112

Khoshnoodi, J., V. Pedchenko, and B.G. Hudson. 2008. Mammalian collagen IV. *Microsc. Res. Tech.* 71:357–370. https://doi.org/10.1002/jemt.20564

King, N., M.J. Westbrook, S.L. Young, A. Kuo, M. Abedin, J. Chapman, S. Fairclough, U. Hellsten, Y. Isogai, I. Letunic, et al. 2008. The genome of the choanoflagellate Monosiga brevicollis and the origin of metazoans. *Nature.* 451:783–788. https://doi.org/10.1038/nature06617

Kramer, J.M. 2005. Basement membranes. *WormBook.* 1:1–15.

Kubota, Y., K. Nagata, A. Sugimoto, and K. Nishiwaki. 2012. Tissue architecture in the Caenorhabditis elegans gonad depends on interactions among fibulin-1, type IV collagen and the ADAMTS extracellular protease. *Genetics.* 190:1379–1388. https://doi.org/10.1534/genetics.111.133173

Lagarrigue, F., C. Kim, and M.H. Ginsberg. 2016. The Rap1-RIAM-talin axis of integrin activation and blood cell function. *Blood.* 128:479–487. https://doi.org/10.1182/blood-2015-12-638700

Li, S., D. Harrison, S. Carbonetto, R. Fassler, N. Smyth, D. Edgar, and P.D. Yurchenco. 2002. Matrix assembly, regulation, and survival functions of laminin and its receptors in embryonic stem cell differentiation. *J. Cell Biol.* 157:1279–1290. https://doi.org/10.1083/jcb.200203073

Li, S., P. Liquari, K.K. McKee, D. Harrison, R. Patel, S. Lee, and P.D. Yurchenco. 2005. Laminin-sulfatide binding initiates basement membrane assembly and enables receptor signaling in Schwann cells and fibroblasts. *J. Cell Biol.* 169:179–189. https://doi.org/10.1083/jcb.200501098

Li, S., Y. Qi, K. McKee, J. Liu, J. Hsu, and P.D. Yurchenco. 2017. Integrin and dystroglycan compensate each other to mediate laminin-dependent basement membrane assembly and epiblast polarization. *Matrix Biol.* 57-58:272–284. https://doi.org/10.1016/j.matbio.2016.07.005

Lilja, J., T. Zacharchenko, M. Georgiadou, G. Jacquemet, N. De Franceschi, E. Peuhu, H. Hamidi, J. Pouwels, V. Martens, F.H. Nia, et al. 2017. SHANK proteins limit integrin activation by directly interacting with Rap1 and R-Ras. *Nat. Cell Biol.* 19:292–305. https://doi.org/10.1038/ncb3487

Liu, J., Z. Wang, A.M.M. Thinn, Y.-Q. Ma, and J. Zhu. 2015. The dual structural roles of the membrane distal region of the α-integrin cytoplasmic tail during integrin inside-out activation. *J. Cell Sci.* 128:1718–1731. https://doi.org/10.1242/jcs.160663

Ma, M., X. Cao, J. Dai, and J.C. Pastor-Pareja. 2017. Basement membrane manipulation in drosophila wing discs affects dpp retention but not growth mechanoregulation. *Dev. Cell.* 42:97–106.e4. https://doi.org/10.1016/j.devcel.2017.06.004

Mango, S.E. 2007. The C. elegans pharynx: a model for organogenesis. *WormBook.* 22:1–26.

Mao, M., M.V. Alavi, C. Labelle-Dumais, and D.B. Gould. 2015. Type IV collagens and basement membrane diseases: cell biology and pathogenic mechanisms. *Curr. Top. Membr.* 76:61–116. https://doi.org/10.1016/bs.ctm.2015.09.002

Matsubayashi, Y., A. Louani, A. Dragu, B.J. Sánchez-Sánchez, E. Serna-Morales, L. Yolland, A. Gyoergy, G. Vizcay, R.A. Fleck, J.M. Heddleston, et al. 2017. A moving source of matrix components is essential for de novo basement membrane formation. *Curr. Biol.* 27:3526–3534.e4. https://doi.org/10.1016/j.cub.2017.10.001

McClatchey, S.T., Z. Wang, L.M. Linden, E.L. Hastie, L. Wang, W. Shen, A. Chen, Q. Chi, and D.R. Sherwood. 2016. Boundary cells restrict dystroglycan trafficking to control basement membrane sliding during tissue remodeling. *eLife.* 5:e17218. https://doi.org/10.7554/eLife.17218

McKee, K.K., S. Capizzi, and P.D. Yurchenco. 2009. Scaffold-forming and Adhesive Contributions of Synthetic Laminin-binding Proteins to Basement Membrane Assembly. *J. Biol. Chem.* 284:8984–8994. https://doi.org/10.1074/jbc.M809719200

McKee, K.K., S.C. Crosson, S. Meinen, J.R. Reinhard, M.A. Rüegg, and P.D. Yurchenco. 2017. Chimeric protein repair of laminin polymerization ameliorates muscular dystrophy phenotype. *J. Clin. Invest.* 127:1075–1089. https://doi.org/10.1172/JCI90854

Morrissey, M.A., and D.R. Sherwood. 2015. An active role for basement membrane assembly and modification in tissue sculpting. *J. Cell Sci.* 128:1661–1668. https://doi.org/10.1242/jcs.168021

Morrissey, M.A., R. Jayadev, G.R. Miley, C.A. Blebea, Q. Chi, S. Ihara, and D.R. Sherwood. 2016. SPARC promotes cell invasion in vivo by decreasing type IV collagen levels in the basement membrane. *PLoS Genet.* 12:e1005905. https://doi.org/10.1371/journal.pgen.1005905

Naegeli, K.M., E. Hastie, A. Garde, Z. Wang, D.P. Keeley, K.L. Gordon, A.M. Pani, L.C. Kelley, M.A. Morrissey, Q. Chi, et al. 2017. Cell Invasion In Vivo via Rapid Exocytosis of a Transient Lysosome-Derived Membrane Domain. *Dev. Cell.* 43:403–417.e10. https://doi.org/10.1016/j.devcel.2017.10.024

Parkin, J.D., J.D. San Antonio, V. Pedchenko, B. Hudson, S.T. Jensen, and J. Savige. 2011. Mapping structural landmarks, ligand binding sites, and missense mutations to the collagen IV heterotrimers predicts major functional domains, novel interactions, and variation in phenotypes in inherited diseases affecting basement membranes. *Hum. Mutat.* 32:127–143. https://doi.org/10.1002/humu.21401

Pastor-Pareja, J.C., and T. Xu. 2011. Shaping cells and organs in Drosophila by opposing roles of fat body-secreted Collagen IV and perlecan. *Dev. Cell.* 21:245–256. https://doi.org/10.1016/j.devcel.2011.06.026

Pöschl, E., U. Schlötzer-Schrehardt, B. Brachvogel, K. Saito, Y. Ninomiya, and U. Mayer. 2004. Collagen IV is essential for basement membrane stability but dispensable for initiation of its assembly during early development. *Development.* 131:1619–1628. https://doi.org/10.1242/dev.01037

Pozzi, A., P.D. Yurchenco, and R.V. Iozzo. 2017. The nature and biology of basement membranes. *Matrix Biol.* 57-58:1–11. https://doi.org/10.1016/j.matbio.2016.12.009

Preibisch, S., S. Saalfeld, and P. Tomancak. 2009. Globally optimal stitching of tiled 3D microscopic image acquisitions. *Bioinformatics.* 25:1463–1465. https://doi.org/10.1093/bioinformatics/btp184

Ramos-Lewis, W., K.S. LaFever, and A. Page-McCaw. 2018. A scar-like lesion is apparent in basement membrane after wound repair in vivo. *Matrix Biol.* 74:101–120. https://doi.org/10.1016/j.matbio.2018.07.004

Randles, M.J., M.J. Humphries, and R. Lennon. 2017. Proteomic definitions of basement membrane composition in health and disease. *Matrix Biol.* 57-58:12–28. https://doi.org/10.1016/j.matbio.2016.08.006

Rasmussen, J.P., S.S. Reddy, and J.R. Priess. 2012. Laminin is required to orient epithelial polarity in the C. elegans pharynx. *Development.* 139:2050–2060. https://doi.org/10.1242/dev.078360

Rasmussen, N.R., D.J. Dickinson, and D.J. Reiner. 2018. Ras-Dependent Cell Fate Decisions Are Reinforced by the RAP-1 Small GTPase in *Caenorhabditis elegans*. *Genetics.* 210:1339–1354. https://doi.org/10.1534/genetics.118.301601

Reiner, D.J., and E.A. Lundquist. 2018. Small GTPases. *WormBook.* 2018:1–65. https://doi.org/10.1895/wormbook.1.67.2

Rual, J.-F., J. Ceron, J. Koreth, T. Hao, A.-S. Nicot, T. Hirozane-Kishikawa, J. Vandenhaute, S.H. Orkin, D.E. Hill, S. van den Heuvel, and M. Vidal. 2004. Toward improving Caenorhabditis elegans phenome mapping with an ORFeome-based RNAi library. *Genome Res.* 14(10b, 10B):2162–2168. https://doi.org/10.1101/gr.2505604

Ruoslahti, E. 1996. RGD and other recognition sequences for integrins. *Annu. Rev. Cell Dev. Biol.* 12:697–715. https://doi.org/10.1146/annurev.cellbio.12.1.697

Schindelin, J., I. Arganda-Carreras, E. Frise, V. Kaynig, M. Longair, T. Pietzsch, S. Preibisch, C. Rueden, S. Saalfeld, B. Schmid, et al. 2012. Fiji: an open-source platform for biological-image analysis. *Nat. Methods.* 9:676–682. https://doi.org/10.1038/nmeth.2019

Sherwood, D.R., and J. Plastino. 2018. Invading, Leading and Navigating Cells in *Caenorhabditis elegans*: Insights into Cell Movement *In Vivo*. *Genetics.* 208:53–78. https://doi.org/10.1534/genetics.117.300082

Shiu, P.K., and C.P. Hunter. 2017. Early Developmental Exposure to dsRNA Is Critical for Initiating Efficient Nuclear RNAi in C. elegans. *Cell Reports.* 18:2969–2978. https://doi.org/10.1016/j.celrep.2017.03.002

Simmer, F., M. Tijsterman, S. Parrish, S.P. Koushika, M.L. Nonet, A. Fire, J. Ahringer, and R.H.A. Plasterk. 2002. Loss of the putative RNA-directed RNA polymerase RRF-3 makes C. elegans hypersensitive to RNAi. *Curr. Biol.* 12:1317–1319. https://doi.org/10.1016/S0960-9822(02)01041-2

Starich, T.A., D.H. Hall, and D. Greenstein. 2014. Two classes of gap junction channels mediate soma-germline interactions essential for germline proliferation and gametogenesis in Caenorhabditis elegans. *Genetics.* 198:1127–1153. https://doi.org/10.1534/genetics.114.168815

Stiernagle, T. 2006. Maintenance of C. elegans. *WormBook.* 11:1–11.

Thinn, A.M.M., Z. Wang, and J. Zhu. 2018. The membrane-distal regions of integrin α cytoplasmic domains contribute differently to integrin

inside-out activation. *Sci. Rep.* 8:5067. https://doi.org/10.1038/s41598-018-23444-w

Timmons, L., and A. Fire. 1998. Specific interference by ingested dsRNA. *Nature.* 395:854. https://doi.org/10.1038/27579

Timmons, L., D.L. Court, and A. Fire. 2001. Ingestion of bacterially expressed dsRNAs can produce specific and potent genetic interference in Caenorhabditis elegans. *Gene.* 263:103–112. https://doi.org/10.1016/S0378-1119(00)00579-5

Tsiper, M.V., and P.D. Yurchenco. 2002. Laminin assembles into separate basement membrane and fibrillar matrices in Schwann cells. *J. Cell Sci.* 115:1005–1015.

Urbano, J.M., C.N. Torgler, C. Molnar, U. Tepass, A. López-Varea, N.H. Brown, J.F. de Celis, and M.D. Martín-Bermudo. 2009. Drosophila laminins act as key regulators of basement membrane assembly and morphogenesis. *Development.* 136:4165–4176. https://doi.org/10.1242/dev.044263

Uspenskaia, O., M. Liebetrau, J. Herms, A. Danek, and G.F. Hamann. 2004. Aging is associated with increased collagen type IV accumulation in the basal lamina of human cerebral microvessels. *BMC Neurosci.* 5:37. https://doi.org/10.1186/1471-2202-5-37

Wang, X., R.E. Harris, L.J. Bayston, and H.L. Ashe. 2008. Type IV collagens regulate BMP signalling in Drosophila. *Nature.* 455:72–77. https://doi.org/10.1038/nature07214

Weber, K.S., L.B. Klickstein, and C. Weber. 1999. Specific activation of leukocyte beta2 integrins lymphocyte function-associated antigen-1 and Mac-1 by chemokines mediated by distinct pathways via the alpha subunit cytoplasmic domains. *Mol. Biol. Cell.* 10:861–873. https://doi.org/10.1091/mbc.10.4.861

Wolfenson, H., I. Lavelin, and B. Geiger. 2013. Dynamic regulation of the structure and functions of integrin adhesions. *Dev. Cell.* 24:447–458. https://doi.org/10.1016/j.devcel.2013.02.012

Yochem, J., and R.K. Herman. 2003. Investigating C. elegans development through mosaic analysis. *Development.* 130:4761–4768. https://doi.org/10.1242/dev.00701

Yurchenco, P.D. 2011. Basement membranes: cell scaffoldings and signaling platforms. *Cold Spring Harb. Perspect. Biol.* 3:a004911. https://doi.org/10.1101/cshperspect.a004911

Yurchenco, P.D. 2015. Integrating Activities of Laminins that Drive Basement Membrane Assembly and Function. *Curr. Top. Membr.* 76:1–30. https://doi.org/10.1016/bs.ctm.2015.05.001

Yurchenco, P.D., and B.L. Patton. 2009. Developmental and pathogenic mechanisms of basement membrane assembly. *Curr. Pharm. Des.* 15:1277–1294. https://doi.org/10.2174/138161209787846766

Zhang, Y., and H. Wang. 2012. Integrin signalling and function in immune cells. *Immunology.* 135:268–275. https://doi.org/10.1111/j.1365-2567.2011.03549.x